Adaptations in wing morphology rather than wingbeat kinematics enable flight in small hoverfly species

Camille Le Roy[1]*, Nina Tervelde[1], Thomas Engels[2], and Florian T. Muijres[1]

[1]**Experimental Zoology Group, Wageningen University, 6709 PG, Wageningen, the Netherlands.**
[2]**CNRS & Aix-Marseille Université**
*Correspondence to: camille.leroy@wur.nl

Abstract

Due to physical scaling laws, size greatly affects animal locomotor ability and performance. Whether morphological and kinematic traits always jointly respond to size variation is however poorly known. Here, we examine the relative importance of morphological and kinematic changes in mitigating the consequence of size reduction on aerodynamic force production for weight support in flying insects, focusing on hovering flight of hoverflies (Syrphidae). We compared the morphology of 28 hoverfly species, and the flight biomechanics and aerodynamics of eight species with body masses ranging from 5 to 100 mg. Our study reveals no significant effect of body mass on wingbeat kinematics among species, suggesting that morphological rather than kinematic changes may compensate for the reduction in weight support associated with an isometric reduction in wing size. Computational Fluid Dynamics simulations confirmed that adaptations in wing morphology drive the ability of small hoverfly species to generate weight support, although variations in wingbeat kinematics between species cannot be completely neglected. We specifically show that smaller hoverflies have evolved relatively larger wings, and aerodynamically more effective wing shapes, to mitigate the reduction in aerodynamic weight support with isometric size reduction. Altogether, these results suggest that hoverfly flight underpins highly specialised wingbeat kinematics, which have been largely conserved throughout evolution; instead, evolutionary adaptations in wing morphology enabled flight of small hoverflies.

Keywords: insect flight, comparative biomechanics, morphometrics, allometric scaling, aerodynamics, CFD, evolution, phylogeny.

Introduction

Evolutionary changes in size are common over the course of animal diversification (Clauset and Erwin, 2008; Hanken and Wake, 1993), strongly impacting many aspects of morphology, physiology, and behaviour. Investigating how changes in body size affect other traits (i.e., scaling) is thus essential to understand the causes

of traits variation in animals. Traditionally rooted in the field of morphology and physiology (Gould, 1966; Hill, 1950; Pélabon et al., 2014), allometric studies have broadened to explore how more complex traits scale with animal size. These include locomotor kinematics (e.g. flight, stride or swimming kinematics, Bejan and Marden, 2006; Riskin et al., 2010), and behaviour (e.g. mating or escape tactics, Dial et al., 2008). Although behavioural or biomechanical traits are often more noisy and challenging to measure, their inclusion in allometric studies is crucial to better understand trait evolution (Cloyed et al., 2021). Indeed, most phenotypes involve both morphological and behavioural traits, each responding in potentially different ways to size variation (Clemente and Dick, 2023). Difference in scaling patterns between body size and other traits is generally most apparent between species, and can be partly explained by neutral divergence during phylogenetic history (Blomberg et al., 2003). Understanding the origin of trait variation among species thus requires controlling for the influence of phylogeny on allometric relationships (Labonte et al., 2016; Peattie and Full, 2007).

In this study, we address the consequences of size variation between species (i.e. evolutionary allometry) and specifically question the relative importance of wing morphology versus wingbeat kinematic changes in mitigating the effect of size on flight ability.

Flight typically combines a suite of morphological and biomechanical traits, providing a relevant context to jointly examine how morphology and locomotor kinematics change with size. Moreover, the physical scaling laws governing flight allow drawing predictions on the scaling of morphology and kinematics in flying animals. These physical laws set both upper and lower bounds on the size of flying animals, resulting from the need to maintain weight-support by producing upward-directed aerodynamic lift forces. In this context, there are two primary limitations for producing these forces: Limitations on (1) the muscular flight motor system, and on (2) the flapping-wing-based aerodynamic thrust-producing system.

(1) Just like terrestrial animals, larger flying animals face increasing constraints on muscle force production as they grow. This limitation arises because muscle force output scales with muscle cross-sectional area, and therefore under isometry it increases at a lower rate than body mass. Consequently, as body size increases, producing the muscle forces for maintaining weight support requires a positive allometry of muscle cross-sectional area (Alexander, 2013). Conversely, smaller animals are not constrained by muscle force production but instead benefit from a favourable surface-to-volume ratio, allowing for a reduction in musculature for locomotion as size decreases.

(2) Next to this constraint on the muscular motor system, flying animals face also constrains stemming from the scaling between their flapping-wing-based propulsion system and body mass. For large flying animals, the aerodynamic lift (L) for weight support scales linearly with the surface area of the wing (S), and quadratically with the flight speed (U_∞) as $L \sim S\, U_\infty^2$ (Norberg, 2007). Under geometric similarity, wing surface area scales with body mass (m) as $S \sim m^{2/3}$ (Schmidt-Nielsen, 1975). Thus, to maintain weight support during flight ($L=mg$, where g is gravitational acceleration), larger flying animals exhibit disproportionately larger wings and tend to fly faster (Norberg, 2012). This positive allometry in wing surface area and flight speed with body mass is needed to generate enough lift to stay in the air.

Smaller flying animals such as insects generally fly slower, and thus air movements over the wing are governed by wing flapping and less so by their forward movement. The aerodynamic lift forces produced by flapping wings scales linearly with the wing's second-moment-of-area (S_2) and quadratically with angular wing speed as $L \sim S_2\, \omega^2$

(Weis-Fogh, 1973). Thus, for small slow flying animals, and particularly during hovering flight, the lift forces required for weight support scale primarily with the wing's second-moment-of-area, relative to the wing hinge (Muijres et al., 2017). For isometry, this second-moment-of-wing-area scales with body mass as $S_2 \sim m^{4/3}$. Because this growth factor of 4/3 is larger than one, a wing's second-moment-of-area decreases at a higher rate than body mass, and therefore wingbeat-induced aerodynamic lift reduces more rapidly than body weight. Thus, to maintain weight support ($mg=L\sim S_2\ \omega^2$), smaller flying animals require disproportionately larger wings, and/or they need to beat their wings at higher wingbeat frequencies or amplitudes, resulting in higher angular speeds of the beating wing. Notably, decreasing size also leads to a drop in Reynolds number, increasing the relative influence of viscous over inertial forces. At the low Reynolds numbers typical of small insects, viscous forces dominate, which may affect how lift is generated during flapping flight (Sane, 2003).

In this study, we aim to test how physical scaling laws cause constrains on the flapping-wing-based aerodynamic thrust-producing system in small insects, and how this drives evolutionary adaptations in wing morphology and wingbeat kinematics. Here, we hypothesize that smaller insects have evolved disproportionately larger wings, and beat their wings at higher wingbeat frequencies, allowing them to maintain weight support despite the detrimental scaling effects of size reduction on their thrust-producing system.

The expected negative allometric scaling in wingbeat frequency with body mass across species is supported by the consistent negative relationship between wingbeat frequency and size observed in most flying animals (Norberg, 2007; Rayner, 1988; Riskin et al., 2010; Tercel et al., 2018). A general trend toward disproportionately larger wings in smaller species is however less striking among species (but see Danforth, 1989; Ellington, 1984a; Outomuro et al., 2013), suggesting that morphological changes in response to size variation are not always straightforward.

Although empirical data often align with expectations drawn from physical laws, the scaling of morphology and kinematic with size can sometimes be challenging to predict. Selective pressures associated with ecological specialisation may influence the evolution of morphology and kinematic, and conflict with the constraints imposed by physical scaling laws. Each component may then adjust for the constraints imposed by weight support in varying degree. For example, changes in morphology have been shown to predominantly mitigate the negative consequences of body size reduction: among hummingbirds, a disproportionate increase in wing area – but little change in wingbeat kinematics – enable weight support among species of different sizes (Skandalis et al., 2017). Similarly, a positive allometry in wing area, but no significant change in wingbeat frequency, was found in relation to body size among species of bees (Duell et al., 2022; Grula et al., 2021). Such discrepancies with the general scaling expectation may point at a particular selective regime maintaining specialised flight kinematics and ability.

Here we focused on an ecologically specialised insect group, the hoverflies, to test if the consequences of size variation are mostly mitigated by changes in wingbeat kinematics or in wing morphology.

Hoverflies (Diptera: Syrphidae) are among the most species-rich groups of nectar-foraging insects and exhibit striking variation in size, ranging from 0.5 mg to over 200 mg (Katzourakis et al., 2001). Despite these large size differences, all adult hoverflies show exceptional hovering abilities. This highly specialised flight behaviour may have been promoted because it plays an important role in mating behaviour: male hoverflies aggregate at specific locations such as under a tree and hover steadily, waiting for passing females to pursue (Gilbert, 1984; Heinrich and Pantle, 1975). Hovering abilities may thus be correlated with mating success (Downes, 1969; Gilbert, 1984).

It may also have been favoured in the context of foraging and navigating around flowers, albeit hovering may not directly relate to feeding as most species land on flowers to feed (Gilbert, 1981). Selection acting on the flight of hoverflies may interfere with general scaling expectations between body mass, wing morphology and wingbeat kinematics.

Here, we study the evolutionary response of wing morphology and wingbeat kinematics to weight support constrains in hovering hoverflies, specifically for small species. Due to the negative scaling with mass of the aerodynamic forces produced by the beating-wing-based aerodynamic thrust-producing system, we hypothesize that tiny hoverflies have evolved relatively large wings or high wingbeat frequencies to maintain weight support during hovering. Because flight behaviour is evolutionarily more labile than morphology (Blomberg et al., 2003), we furthermore hypothesize that adaptations in wingbeat kinematics prevail over wing morphological adaptations. Alternatively, if selection for strong hovering performance is limiting kinematic flexibility, we expect weight support to be maintained across sizes through adaptations in wing morphology rather than in wingbeat kinematics.

We test these hypotheses by examining the scaling relationships between wing morphology and body mass in 28 hoverfly species ranging from 3 to 132 mg, and conjointly assessing how wing morphology and wingbeat kinematics scale with body mass for eight species ranging from 5 to 100 mg. We then combined computational fluid dynamic simulations with quasi-steady aerodynamic modelling to estimate aerodynamic forces produced in hovering flight. Based on this, we determined how the relative changes in wingbeat kinematics and wing morphology contribute to producing weight support during hovering flight of hoverflies.

Material and methods

Collecting and identifying hoverflies

We quantified body and wing morphology in 28 hoverfly species, of which we collected eight species in the wild and twenty from museum specimens at the Naturalis Biodiversity centre (Leiden, the Netherlands). The wild caught live hoverflies were also used for flight experiments, to quantity their wingbeat kinematics during hovering flight (Figure 1).

From the museum collection, we sampled 74 individual specimens, aiming to include two males and two females per species whenever possible. This resulted in 4.2±1.7 individuals per species (mean±standard deviation). Museum specimens were selected to maximize both phylogenetic coverage and size range. The eight hoverflies from the wild were collected in September 2022 on the campus of Wageningen University, the Netherlands (51°59’01.0”N 5°39’32.7”E; ca. 10 m). We captured a total 44 individuals, resulting in a sample size of 5.5±2.9 individuals per species. Flies were captured with hand-held nets and brought in the lab to record their flight within an hour after capture, after which morphology was quantified.

The wild species were first distinguished visually, but their species identity was subsequently ascertained using DNA barcoding. This was done by sending a piece of leg of each individual to the Canadian Centre for DNA Barcoding (CCDB), where barcoding was performed following standard automated protocols of the BOLD Identification System (http://www.boldsystems.org/) (Ratnasingham and Hebert, 2007). Sequenced DNA was

then compared with a reference library to establish a species match. Sexes were determined visually using criteria from Gilbert (2015).

Flight experiments

The flight experiments were carried out in a custom-built octagonal flight arena made of transparent Plexiglas (50×50×48 cm, height×width×length; Figure 2A) (Cribellier et al., 2022). Stereoscopic high-speed videos were recorded using three synchronised high-speed cameras (Photron FASTCAM SA-X2), equipped with Nikon Sigma 135 mm lenses, and recording at a temporal resolution of 5000 frames s^{-1}, a spatial resolution of 1084×1084 pixels, and a shutter speed of 1/10000 s. The cameras were positioned around the arena to provide a top view, and inclined left and right-side view of the flying insects, which resulted in a zone of focus of approximately 12 cm^3 in the centre of the arena in which body and wing movement were in view and in focus of all three cameras. To increase contrast and therefore facilitate subsequent tracking, the cameras were back-lit using three infrared light panels, placed behind the bottom and lower side walls of the octagon arena, opposite each camera (Figure 2A).

Prior to filming, the stereoscopic camera system was calibrated with the direct linear transformation (DLT) technique (Hartley and Sturm, 1995), by digitising a wand of 2.8 cm long moved throughout the zone of focus of the cameras. To track the wand movement, we trained an artificial neural network using the pose estimation Python library DeepLabCut (Nath et al., 2019), achieving a test error of 3.1 pixels. Computation of the DLT coefficients was then done using the MATLAB program easyWand (Theriault et al., 2014). The calibration root mean square error was 1.21 pixels.

During the flight experiment, all the individuals from a single species were released together in the arena to increase the probability that an individual flew through the intersecting fields of view of the three cameras. Most individuals tended to remain on the sidewalls, occasionally making short flights across the arena. For each species, the filming experiment was carried out until a minimum of five suitable flight sequences were obtained, whenever possible. A suitable sequence was defined as a flying individual clearly crossing the intersecting fields of view. Although this procedure facilitated the recording, this prevented identifying which specific individual or sex was recorded flying, leaving open the possibility of recording the same individual multiple times. Note that this approach aimed at estimating the average wingbeat kinematics per species as we could not directly assign flight measurements at the individual level.

Wingbeats selection

First, we determined the flight speed throughout each recorded flight sequence. We did this by tracking the hoverfly body centre, estimated from the mean position between the head and abdomen extremities, throughout the flight sequence (mean duration of the tracked trajectories = 0.13±0.11 sec) using a trained DeepLabCut neural network (Nath et al., 2019) (test error: 6.3 pixels). From this, we calculated flight speed using a central temporal differentiation scheme. Based on these speed data, we selected flight sequences with the lowest average speed and, within each sequence, identified the wingbeat occurring during the slowest part of the trajectory. For this selection process, we only included the flight trajectory sections in which the hoverfly was flying straight at a low climb angle, to prevent possible variation in wingbeat kinematics stemming from flight manoeuvres. We digitised

a minimum of three wingbeats per species, each taken from a different flight sequence. For six of the species we tracked three wingbeats, and for two species (*Melanostoma mellinum* and *Sphaerophoria scripta*) we tracked six wingbeats. Note that our experiment did not allow capturing perfect hovering flight sequences (i.e. flight speed = 0 m.s^{-1}) but aimed at getting as close as possible to this flight mode. This was evaluated using the advance ratio (see next section).

Quantifying wingbeat kinematics

We quantified the wing movement using the manual stereoscopic video tracker *Kine* in MATLAB (Fontaine et al., 2009; Fry et al., 2003) originally designed to track the wingbeat kinematics of fruit flies. The tracker was tailored to hoverflies by building wing models matching the wings of the studied hoverfly species. Wing models were obtained by digitising the wing outline on high-resolution photographs and consisted of 41 2D coordinates representing the wing shape, with the known hinge and tip positions. To reduce complexity, wings were considered as rigid flat plates, although real hoverflies wings endure deformations during the wing stroke (Walker et al., 2010).

We tracked the wingbeat kinematics on down-sampled videos (from 5000 to 2500 frames s^{-1}), as this preserved high enough temporal resolution to capture the wing movement (n=27±5 frames per wingbeat). The tracking provided us with the position and orientation of the body and wings in each consecutive video frame. The position and orientation of the body were defined in the world reference frame, as a 3D position vector (**X**=[x,y,z]) and the consecutive Euler angles body yaw, pitch and roll. The angular orientation of the wings was expressed in the hoverfly body reference frame (Muijres et al., 2014) (Figure 2B), as Euler angles relative to the stroke plane: the stroke angle (ϕ), deviation angle (η) and rotation angle (θ) of each wing (Figure 2B). The stroke plane of each wing was defined as the plane at a 45° angle to the long axis of the body passing through the hinge position of that wing. The three wing kinematics angles (stroke, deviation and rotation angle) were measured separately on the left and right wing and then averaged between the two wings. The time history of the averaged angles was then fitted with a 4th order Fourier series for all three angles (Muijres et al., 2014), and their temporal derivatives were computed (i.e. stroke, deviation and rotation rate). We estimated the absolute angular speed of the beating wing as $\omega = \sqrt{\dot{\phi}^2 + \dot{\eta}^2}$ where $\dot{\phi}$ and $\dot{\eta}$ are the stroke rate and deviation rate, respectively. The angle of attack (α) was computed as the angle between the wing plane and the velocity vector of the wing (Figure 2B).

Based on the temporal dynamic of the wing kinematics angles, we derived the following wingbeat-average kinematics parameters: wingbeat frequency, defined as f=1/Δt, where Δt is the duration of the wingbeat; wing stroke, deviation, and rotation amplitudes, defined as A_ϕ=|ϕ_{max} −ϕ_{min}|, A_η=|η_{max} −η_{min}|, and A_θ =|θ_{max} −θ_{min}|, respectively; we estimated the wingbeat-average angular speed as $\bar{\omega} = 2\, f\, A_\phi$; we estimated the mean angle-of-attack $\bar{\alpha}$ as the mean value at mid forward and backward wing stroke, where aerodynamic force production is close to maximum (Tian et al., 2013).

We quantified the wingbeat-average body kinematics during each wingbeat using the mean flight speed, climb angle, and the pitch angle of both body and stroke-plane. Flight speed **U** was estimated as the temporal derivative of body positions, and climb angle as γ_{climb}=atan(U_{ver}/U_{hor}), where U_{ver} and U_{hor} are the vertical and horizontal component of the flight velocity. Body pitch angle β_{body} was calculated as the angle between the body axis and the

horizontal. The equivalent stroke-plane pitch angle was defined as the pitch angle of the stroke plane relative to the horizontal, calculated as $\beta_{stroke\text{-}plane}=\beta_{body}-45°$.

To verify whether the studied wingbeats were representative of the overall recorded flight behaviour, we calculated the mean wingbeat frequency over the full flight sequence as $\hat{f}=n_{wingbeats}/T_{sequence}$, where $n_{wingbeats}$ and $T_{sequence}$ are the number of wingbeats in a sequence and the sequence duration, respectively. This mean wingbeat frequency was then compared with that of the studied wingbeats. To estimate whether the analysed wingbeats were representative for hovering flight we calculated the advance ratio of all wingbeats as $J = U/(\bar{\omega}\, R)$, where R is the span of a single wing. Hovering is generally defined as flight with advance ratios $J<0.1$, i.e. when the forward flight speed is less than 10% of the wingbeat-induced speed of the wingtip (Ellington, 1984a).

Finally, although hoverfly flight speed was minimised in the wingbeat selection procedure, remaining variation in body kinematics may still affect the wingbeat kinematics and therefore confound with changes in wingbeat kinematics resulting from scaling effect. We therefore assessed if the flight kinematics metrics flight speed and climb angle affected wingbeat kinematics by performing multiple regression analyses. Here, each wingbeat kinematic metric was treated as dependent variable and flight speed and climb angle as model effects.

Quantifying morphology

We quantified body and wing morphology in both the wild-caught hoverflies and the museum specimens. After being filmed flying, wild-caught individuals were sacrificed by freezing them at -20°C, and weighed with a resolution of 0.1 mg using an analytical balance (XSR204 Mettler Toledo). Wings were then detached from the body and photographed using a digital microscope (Zeiss Stemi SV11). From the museum collection, we only selected specimens with properly flattened (i.e., non-folded) wings, and photographed them using a Nikon D600 camera equipped with a 60mm lens. Here, we photographed the complete animal from above, and the separate wing by it placing parallel to the camera lens. We estimated body mass of museum specimens using the correlation between thorax width and the fresh mass in the wild caught specimens (Figure S1).

From the wing photographs of both the wild and museum specimens, we measured the primary wing morphology parameters using WingImageProcessor in MATLAB (available at https://biomech.web.unc.edu/wing-image-analysis/). These include single-wing area S, wingspan R, mean wing chord $\bar{c}$, and second-moment-of-area S_2. From these we calculated weight-normalised wingspan as $R^*=R/m^{1/3}$, and the normalised second-moment-of-area as $S_2^* = S_2/(R^3\bar{c})$. The weight-normalized wingspan is a parameter describing relative wingspan, and the normalised second-moment-of-area is a non-dimensional parameter defining wing shape changes independent of changes in wing size. Both parameters allowed us to identify variations in relative wingspan and relative wing shape between species of different sizes, respectively.

Next, we used a landmark-based geometric morphometric method to quantify more precisely the variation in wing shape between species (Bookstein, 1997). Wing shape outline was determined using 300 semi-landmarks equidistantly spaced along the wing outline. Semi-landmarks are commonly used to describe curvy shapes such as wing outlines, which lack typical identifiable landmarks (Gunz and Mitteroecker, 2013). Semi-landmarks are allowed to slide along the curve to establish geometric correspondence (Gunz and Mitteroecker, 2013). After this alignment, the landmarks are treated as regular ones in subsequent analyses. We placed one fixed landmark at

the base of the wing, fixing the overall landmark configuration with respect to this homologous position available for all specimens. All landmarks were digitised using *TpsDig2* (Rohlf, 2015). Wing outlines were superimposed by performing a generalised Procrustes analysis (Rohlf and Slice, 1990) using the *geomorph* R package (Adams and Otárola-Castillo, 2013). This procedure isolates the shape information from the extraneous variations, namely: the size, position, and orientation. To visualize wing shape variation, we then performed a phylogenetic Principal Component Analysis (phyloPCA) on the superimposed coordinates using the *phytools* R package (Revell, 2012). Shape changes carried on the PCA axes were visualised using the *plotRefToTarget* function in *geomorph*.

To assess the strength of morphological sexual dimorphism and whether it may interfere with interspecific differences, we tested the effect of species and sex on the morphological parameter using analyses of variance (ANOVAs).

Testing the influence of phylogeny on flight kinematics and morphological traits

To assess whether shared evolutionary history among the studied species influenced variation in morphology and wingbeat kinematics, we tested if closely related species showed more similar values in the measured parameters than distantly related ones. This was done by computing phylogenetic signals with the Blomberg's K-statistics (Blomberg et al., 2003) on each morphological and flight parameters using the R package *phytools* (Revell, 2012). Furthermore, we accounted for the effect of phylogeny when assessing the scaling relationships between size and traits using Phylogenetic Generalized Least Squares (PGLS) regression (Symonds and Blomberg, 2014). For the PGLS regressions, we assumed a Brownian motion model of evolution, and the model parameters were estimated using maximum likelihood. Tests were performed on the mean values per species using the most recent phylogeny of hoverflies (Wong et al., 2023). The phylogeny was pruned to align with our sample of 28 species for the morphological analysis and further pruned to include only the eight species used in the flight analysis.

Modelling the aerodynamics of hoverfly flight

To estimate how changes in wing morphology and wingbeat kinematics affect the aerodynamic forces required for flight, we modelled the aerodynamic vertical force produced by flapping wings in hovering flight using a simplified quasi-steady approach as (Ellington, 1984b)

$$\bar{F} = \frac{1}{2}\,\rho\, S_2\, \bar{\omega}^2\, \bar{C}_F\,, \tag{1}$$

where $\bar{F}$ is the wingbeat-average upward-directed aerodynamic lift force produced by a beating wing. This aerodynamic force thus varies quadratically with the angular speed of the beating wing ($\bar{\omega}^2$), and linearly with air density (ρ), the second-moment-of-area of the wing (S_2), and the lift force coefficient ($\bar{C}_F$).

The second-moment-of-area S_2 is the only morphological parameter in this equation, thus capturing how wing morphology affects aerodynamic force production, from a first principle. But this second-moment-of-area parameter combines both wing size and shape characteristics (i.e., wing area and its distribution over the spanwise axis (Ellington, 1984c)). To disentangle the respective effect of wing shape and size on aerodynamic force production, the second moment-of-area can be decomposed as $S_2 = S_2^*\, R^3\, \bar{c}$, where R is the wingspan, $\bar{c}$ is the mean wing chord, and S_2^* is the normalised second-moment-of-area of the wing. Here, wingspan and average

wing chord are size dependent parameters; the non-dimensional second-moment-of-area describes wing shape as the distribution of area along the spanwise wing axis, independent of wing size.

The lift force coefficient depends on the angle-of-attack, and for fruit flies this dependency can be modelled as $C_F = \sin(\alpha)\, C_{F\alpha}$, where $C_{F\alpha}$ is the angle-of-attack-specific lift force coefficient (Dickinson and Muijres, 2016). For hoverflies, we here assume a similar scaling of lift with angle-of-attack. Both angular speed (ω) and the angle-of-attack (α) of the beating wing are wingbeat kinematics parameters that directly affect aerodynamic force production. A flying insect can vary the angular speed of its beating wings by changing both its wingbeat frequency f and wing stroke amplitude A_ϕ, as angular speed scales linearly with the product of these ($\omega \sim f\, A_\phi$). The decomposed model for estimating the effect of wing morphology and kinematics of aerodynamic lift force production in flapping insect flight is thus

$$\bar{F} = \frac{1}{2}\, \rho\, R^3\, \bar{c}\, S_2^*\, \left(f\, A_\phi\right)^2 \sin(\bar{\alpha})\, \bar{C}_{F\alpha}. \tag{2}$$

We used this model to decompose the relative effect of variations in wingbeat kinematic and wing morphology between species on aerodynamic force production.

Physical scaling of kinematics and morphology parameters with size

In hovering flight, the aerodynamic vertical force F should equal the weight of the animal. Thus, to maintain weight support among different sizes of hoverflies, the aerodynamic force should scale linearly with body mass. This cannot be achieved through isometric scaling, i.e. the expected scaling if geometric similarity is preserved.

For isometric scaling of morphology with mass, all length parameters scale with mass as $l_{iso} \sim m^{1/3}$, resulting in an isometric scale factor under morphological similarity a_{sim}=1/3. As a result, the morphological parameters of interest scale with body mass as $R \sim m^{1/3}$, $\bar{c} \sim m^{1/3}$ and $S_2^* \sim m^0$, and thus both S_2 and F scale with body mass as $F \sim S_2 \sim m^{4/3}$ (see supplementary text for detailed derivation). This value is larger than one, and so with an isometric reduction in size the aerodynamic force for weight support reduces more quickly than body mass. Thus, compared to large species of hoverflies, small species need relatively larger wings or adjust their wingbeat kinematics to maintain weight support.

For the wingbeat kinematics, we define kinematic similarity when the kinematics parameters of interest do not scale with size, and should thus remain constant across body mass. Specifically, wingbeat frequency (f), stroke amplitude (A_ϕ), angular speed (ω), and angle of attack (α) are all expected to scale under kinematic similarity as $f \sim m^0$, $A_\phi \sim m^0$, $\omega \sim m^0$, and $\alpha \sim m^0$, respectively. As hoverflies become smaller, deviations from this kinematic similarity might occur to adjust for the reduction in weight support due to isometric size reduction.

Using our aerodynamic force model (Eqns 1-2) we can estimate how the combination of wing morphology and wingbeat kinematics should scale with size, while maintaining weight support for hovering flight across sizes ($F=mg$). Here, we do so for two extreme cases: (1) weight support is maintained across sizes using allometric scaling of wing morphology only, and thus wingbeat kinematics are kept constant (kinematic similarity); (2) weight support is maintained across sizes using allometric scaling of wingbeat kinematics, while wing morphology scales isometrically.

(1) To maintain weight support with non-varying wingbeat kinematics, the second-moment-of-area should scale linearly with body mass ($S_2 \sim m$), resulting in negative allometry of S_2 relative to body mass ($S_2 \sim m^1 < m^{4/3}$). This could be achieved by negative allometric scaling in the wingspan, mean chord or normalised second-moment-of-area ($R < m^{1/3}$, $\bar{c} < m^{1/3}$ or $S_2^* < m^0$), or a combination of these. To maintain weight support via negative allometric scaling of only one of these three metrics, while the others scale isometrically, then these should scale with mass as $R \sim m^{2/9}$, $\bar{c} \sim m^0$ or $S_2^* \sim m^{-1/3}$ (see supplementary text for detailed derivations).

(2) To maintain weight support via allometric scaling of kinematics, while wing morphology scales isometrically ($S_2 \sim m^{4/3}$), the angular speed of the beating wing should scale with body mass as $\omega \sim m^{-1/6}$ (see supplementary text for detailed derivations). Again, a hovering hoverfly could achieve this using a comparative adjustment in wingbeat frequency or wing stroke amplitude ($f \sim m^{-1/6}$ or $A_\phi \sim m^{-1/6}$, respectively), or a combination of both ($\omega \sim f\, A_\phi \sim m^{-1/6}$). Furthermore, the animal could adjust the aerodynamic force vector using an equivalent adjustment in the wing angle-of-attack ($\sin(\alpha) \sim m^{-1/6}$).

To examine how wing morphology and wingbeat kinematics scales with body mass, and whether this scaling is allometric, we regressed the morphology and wingbeat-average kinematics metrics in Eqns 1-2 (S_2^*, $\bar{c}$, R, $\overline{\omega}$, f, A_ϕ and $\overline{\alpha}$) against the body mass (m), using Phylogenetic Generalized Least Square (PGLS) regressions (Symonds and Blomberg, 2014). Measurements were all $\log_{10}$-transformed prior to the regression analysis. For each morphology and kinematics metric, we tested if the observed scaling factor significantly deviates from isometry or kinematic similarity, respectively ($R \sim m^{1/3}$; $\bar{c} \sim m^{1/3}$; $S_2^* \sim m^0$ and $\overline{\omega} \sim m^0$; $f \sim m^0$; $A_\phi \sim m^0$; $\overline{\alpha} \sim m^0$, respectively), by verifying if its 95% confidence intervals excluded the similarity slope.

To better visualize variations in wing shape and size relative to body mass among species, we scaled all wings with the length-scale for isometry ($l_{iso} \sim m^{1/3}$) and calculated the corresponding weight-normalised wingspan as $R^* = R/m^{1/3}$. We performed additional PGLS regressions to test if other kinematic adjustments were associated with changes in body mass, in addition to the ones considered in the aerodynamics model (Eqns 1-2). This includes regressions of body mass versus the amplitudes of the additional measured wingbeat kinematics angles (A_η, A_θ), and the corresponding peak angular rates ($\dot{\phi}_{\mathrm{peak}}$, $\dot{\eta}_{\mathrm{peak}}$, $\dot{\theta}_{\mathrm{peak}}$).

The relative contribution of allometric scaling in wing morphology and kinematics to maintaining weight-support across sizes

In this study, we hypothesize that small hoverflies have evolved relatively large wings or high wingbeat frequencies to maintain weight support during hovering. Furthermore, we hypothesize that adaptions in wingbeat kinematics will prevail over adaptions in wing morphology, as kinematics is more flexible than morphology (Blomberg et al., 2003). Alternatively, if selection for specialised hovering flight is limiting kinematic flexibility, weight support in small hoverflies might be achieved primarily through changes in wing morphology rather than in wingbeat kinematics.

We tested these hypotheses by assessing how the potential allometric changes in morphology and kinematics contribute to maintaining weight support across the studied range of hoverfly sizes. We did so by comparing, for each relevant morphological and kinematics parameter, its observed mass-specific allometric scaling factor (a_{allo}) with both the scaling factor for morphologic or kinematic similarity (a_{sim}), and the scaling factor for achieving

weight support fully by allometric scaling of only that parameter (a_{ws}). Hereby, we calculated the relative allometric scaling factor for weight-support as

$$a^* = \frac{a_{\text{allo}} - a_{\text{sim}}}{a_{\text{ws}} - a_{\text{sim}}} \cdot 100\%. \quad (3)$$

This parameter defines the percentage of which the observed allometric scaling of the specific morphological or kinematics parameter contributes to maintaining weight support during hovering flight, across the studied size range of hoverflies (see supplementary text for detailed derivations).

Computational fluid dynamics simulations

We performed Computational Fluid Dynamics (CFD) simulations to quantify aerodynamic force produced by the different flying hoverfly species. These simulations allowed us to explicitly quantify the effect of size, wingbeat kinematics and morphology on aerodynamic force production. Furthermore, we used the CFD results to test the validity of our simplified quasi-steady aerodynamic model (Eqns 1-2).

Each simulation was performed with a single rigid, flat wing with species-specific contours, and the averaged wingbeat kinematics across all species. The computational domain was $8R \times 8R \times 8R$, and we simulated three consecutive wingbeat cycles. The wing has a thickness of 0.0417 R. We assumed hovering flight mode, so no mean inflow was imposed ($U_\infty = 0$ m s^{-1}).

We performed the simulations using our in-house open-source code WABBIT (Wavelet Adaptive Block-Based solver for Insects in Turbulence) (Engels et al., 2022, 2021). The computational approach is based on explicit finite differences that solve the incompressible Navier–Stokes equation, in an artificial compressibility formulation. Wavelets are used to dynamically adapt the discretisation grid to the actual flow at every given time t. This allows us to focus the computational effort where it is required to ensure a given precision, while the grid is significantly coarsened wherever possible. Starting from a coarse base grid, we allow up to seven refinement levels, each one refining the grid by a factor of two. In this work we use the Cohen-Daubechies-Feauveau wavelet CDF42. The grid is composed of blocks of identical size with B_s=22 points in all three spatial directions, yielding an effective maximum resolution of 352 points along the wingspan. An additional simulation with eight refinement levels confirmed validity of our results.

As demonstrated in numerous validation tests, obtained numerical data can be regarded as quasi-exact in the sense that they are equivalent to an experiment with identical geometry and kinematics. More details on the code can be found in Engels et al., (2021); the required parameter files to reproduces the simulations presented here can be found in the supplementary information. To accelerate the computation, each simulation used up to 600 CPU cores with 2.7 TB of memory in total.

From a fluid dynamics point of view, changing wing length R or wingbeat frequency f changes the Reynolds number Re (Batchelor, 1967). For each species, we performed a simulation using two different values for Re, one at the average Reynolds number for all species, and a second at the species-specific Reynolds number. This was initially done to separate the effect of Reynolds number and wing shape between species. The non-dimensional aerodynamic force was however very similar in both cases, hence the influence of Reynolds number is negligible.

In general, the range of Reynolds numbers for the studied hoverfly species is rather narrow (Re ∈ [324,1310]). We finally assessed the contribution of interspecific variation in wingbeat frequency to force production by rescaling all aerodynamic forces with the square of the species-specific and average wingbeat frequency ratio $(f/\bar{f})^2$.

The relative contribution of variations in wing size, shape and kinematics to aerodynamic force production

By combining the CFD simulation results with our aerodynamic force model (Eqns 1-2) and our physical scaling law analysis, we assessed the relative contribution of changes in wing size, shape and kinematics between the studied species on the aerodynamic force production required for weight support.

Because wingbeat kinematics were found to vary little across species and to be uncorrelated with body mass, we based this analysis on the average wingbeat kinematics of all species combined (see CFD methods above for details). We did assess the contribution of interspecific variation in wingbeat frequency on aerodynamic force production, as this varied most between species. We did so by rescaling all aerodynamic forces from CFD with the square of the species-specific and average wingbeat frequency ratio $(f/\bar{f})^2$. According to the quasi-steady model, the vertical aerodynamic force from CFD should scale with the product of the wing's second-moment-of-area and angular wing speed squared (Eqn 1: $F \sim S_2\ \omega^2$). The angular wing speed scales linearly with wingbeat frequency ($\omega \sim f$), and the second-moment-of-wing-area can be decomposed into the wing size and shape parameters wing span, mean chord and normalised second-moment-of-area as $S_2\ = R^3\ \bar{c}\ S_2^*$ (Eqn 2).

In our CFD-based scaling analysis, we first tested the validity of our aerodynamic model (Eqns 1-2) by correlating the CFD-based vertical aerodynamic force with the product of second-moment-of-area and wingbeat-average angular speed squared (Eqn 1: $F \sim S_2\ \bar{\omega}^2$). For this, we used an Ordinary Least Squares (OLS) regression on the log-transformed data to quantify the scaling factor between these metrics. We used the regression statistics to test whether the CFD-based force scaled significantly with $S_2\ \bar{\omega}^2$ (with cut-off at P<0.05). Based on these results, we then quantified the corresponding relative allometric scaling factor a^* (Eqn 3), to assess how allometric scaling of $S_2\ \bar{\omega}^2$ contribute to changes in aerodynamic force production at different sizes.

Secondly, we estimated the relative contribution of the primary variables in $S_2\ \bar{\omega}^2$ to aerodynamic force production, being second-moment-of-area and wingbeat frequency. We did so by using the same approach as described above, by first determining the scaling of CFD-based aerodynamic force with second-moment-of-area and wingbeat frequency, and secondly by estimating the corresponding relative scaling factors a^*. Finally, we used this approach to estimate the relative contributions to aerodynamic force production of the S_2-components: wingspan, mean chord length, and normalized second-moment-of-area.

This combined analysis allowed us to estimate the relative contribution of the various morphology and kinematics metrics to variations in vertical force production for weight-support across sizes, and test how hoverflies might have adapted specific wing morphology and kinematics parameters to maintain weight support across sizes. Moreover, comparing the calculated weight-support percentages in our model with 100% for full weight support, allowed us to test the validity of our analysis approach and aerodynamic force model.

Results

In this study, we examined the morphology of 28 hoverfly species, with body masses ranging from 3 to 132 mg. Among them, we analyzed the hovering flight biomechanics and aerodynamics of eight species, with body masses

ranging from 5 to 100 mg. The sampled species were well spread throughout the phylogeny of hoverflies (Figure 1). Among the eight species for which we studied flight biomechanics, body mass variation was unevenly distributed. Only one species, *Eristalis tenax*, weighed more than 50 mg, while the two closely related species *Syrphus nigrilinearus* and *Eupeodes nielseni* had highly similar body masses (Figure 1).

Sexual dimorphism in morphological traits was observed in body mass, wing chord, and wing second-moment-of-area (Table S1). However, the direction of this difference varied across species, with males exhibiting larger values in some cases and females in others. Interspecific difference in morphology was much stronger (Table S1), making sexual dimorphism negligible in comparison. While sexual differences in flight kinematics could not be assessed in this study (see Methods), they are likely to be similarly outweighed by interspecies variation.

When testing the phylogenetic signal on wing morphology and body size among the 28 studied species, we detected a significant effect of phylogeny on all traits except for the second-moment-of-area. In contrast, the effect of phylogeny on flight, tested on eight species, was non-significant for all flight traits (Table S2).

No correlation between wingbeats kinematics and body mass

We quantified a total of 33 wingbeats across eight hoverfly species, including at least three wingbeats per species (Figures 2 and 3). The wingbeat frequencies of the studied wingbeats were highly correlated with the average wingbeat frequency calculated on the entire flight sequence ($\bar{f}$=186±43 Hz; $\hat{f}$=178±40 Hz; mean±standard deviation; *n*=33 flight sequences; r=0.98, P<0.001). Here, the number of wingbeats per flight sequence was 26±28. This suggests that the digitised wingbeats reliably reflect those of the full flight sequences. Furthermore, the mean advance ratio for the digitised wingbeats was below the generally accepted threshold of 0.1 ($\bar{J}$=0.08±0.02), confirming that the hoverflies were operating approximately in a hovering flight mode (Ellington, 1984a).

The eight hoverfly species exhibited similar wingbeat kinematics (Figures 2 and 3A-E). Here, they all moved their wings forward and backwards sinusoidally within the stroke plane (Figure 3A), with a wing stroke amplitude of A_ϕ=100°±18° (Figure 3H). Movements out of the stroke-plane, as expressed by the deviation angle, are minimal (Figure 3B). Therefore, the oscillatory angular speed of the wingbeats (Figure 3D) is primarily caused by the wing stroke movement, and peak at approximately $5°\times10^4$ s^{-1} (Figure 3F). During the majority of each wingbeat (forward and backward wing stroke), the wing operates at approximately constant wing rotation angle and angle-of-attack (Figs 3C and 3E, respectively). At the end of the forward and backward wing stroke, the wings rapidly supinate and pronate, respectively. This causes the wing to flip upside down at stroke reversal, allowing it to operate again at the constant wing angle-of-attack of $\bar{\alpha}$=42°±10° (Figure 3I). The hoverflies flew with a mean body pitch angle of β_{body}=30°±16°. The corresponding pitch angle of the wing stroke-plane was $\beta_{stroke\text{-}plane}$=−15°±16°, showing that these hoverflies hover with an inclined stroke-plane.

The temporal dynamics of wingbeat kinematics was apparently not associated with variation in body mass (Figures 3A-E). Accordingly, none of the derived wingbeat-average wing kinematics parameters varied significantly with body mass, although a small negative trend was observed for the wingbeat frequency (Table 1, Figures 3F-I and S2). These include the parameters that directly affect aerodynamic force production (Eqn 1-2, wingbeat-average angular speed $\bar{\omega}$, angle-of-attack $\bar{\alpha}$, stroke amplitude A_ϕ and wingbeat frequency *f*), and the additionally

estimated wingbeat kinematic parameters (rotation amplitude A_θ, deviation amplitude A_η, and peak stroke rate $\dot{\phi}_{\mathrm{peak}}$, rotation rate $\dot{\theta}_{\mathrm{peak}}$ and deviation rate $\dot{\eta}_{\mathrm{peak}}$) (Table S4).

Furthermore, variations in wingbeat kinematics were little affected by the flight kinematics metrics flight speed and climb angle (Table S3). Only flight speed had a positive significant effect on the angular speed of the beating wings, suggesting that faster flying hoverflies beat their wings at higher angular speeds. When controlling for this effect of flight speed on angular wing speed, the regression between angular wing speed and body mass remained non-significant (r^2=0.02; P=0.41). Additionally, flight speed was not correlated with body mass (r^2=0.01, P=0.43).

These combined results suggest that variation in wingbeat kinematics between species cannot be explained by the demands of maintaining weight support throughout (isometric) size changes (Figure 3). Allometric adjustments for maintaining weight support across sizes among hoverfly species thus more likely occur through changes in wing morphology.

Wing morphology covaries with body mass

Wing morphology strongly covaried with body mass: the wing's second-moment-of-area (S_2), span (R), mean chord ($\bar{c}$), and non-dimensional second-moment-of-area (S_2^*) all significantly correlated with body mass (Figure 4, see also Figure S3). Covariation between the wing morphological parameters and body mass all deviated from the isometric expectation, except for mean chord (Table 1, Figure 4). Second-moment-of-area, wingspan and S_2^* all showed a significant negative allometry, i.e., they were all disproportionately larger in smaller species (Figure 4A-C, Table 1). Scaling of the second-moment-of-area with size differed the most from isometric scaling for morphological similarity (a_{allo}=1.01 versus a_{sim}=1.33) and almost perfectly aligned with the scaling for metric-specific weight-support (a_{ws}=1). The corresponding relative scaling factor confirms this (Eqn 3), as it is close to 100% (a^*_{S2}=98%; Figure 4E). This suggests that hoverfly species of different size should be able to maintain weight-support during hovering flight almost purely through variations in the second-moment-of-area. By estimating the relative scaling factors of the various morphological parameters that compose the second-moment-of-area (Figure 4F), we find that adaptations in wingspan contribute the most to the variations in second-moment-of-area (a^*_R=71%; a^*_c=12%; $a^*_{S2^*}$=5%, Figure 4F). Allometric scaling in the non-dimensional second-moment-of-area had the smallest yet significant effect, indicating a small but notable change in wing shape associated with body mass variation.

Our phylogenetic geometric morphometrics analysis revealed two main axes of wing shape variation among the studied species associated with the principal components PC1 and PC2, explaining 69.21% and 14.64% of the variation, respectively (Figure S4 and S5). Shape variation carried on PC1 was correlated with the S_2^* (r=-0.49; P=0.009) as well as body mass (r=0.55; P=0.002) (Figure 5), depicting the changes in wing shape associated with body mass variation among hoverflies species. This change in S_2^* reflects a wing surface area mostly located distally in smaller species, whereas most wing surface area is located near the wing base in larger hoverflies species (Figure 5).

The combined correlative and morphometrics analyses thus shows that as their size decreases, hoverflies exhibit relatively larger wings that are also shaped such that their normalised second-moment-of-area is

maximized (Figures 4 and 5). These combined morphological adaptations allow smaller hoverflies to maintain in-hovering weight-support without the need to adjust their wingbeat kinematics.

Aerodynamic modelling confirms the main role of wing morphology for weight support

Because among the eight hoverfly species, wingbeat kinematics did not vary significantly with body mass (Table 1), we performed all CFD simulations with the average wingbeat kinematics of all species combined (Figure 6A). We did vary the wing shape and size between species (top row of Figure 6), and we modelled aerodynamic force production with both the species-specific wingbeat frequency and mean wingbeat frequency of all species combined (Figure 6B).

The resulting aerodynamic forces differed between species mostly in magnitude, but the temporal dynamics of force production were strikingly similar (Figure 6C and S6). For all species, the temporal dynamics of the vertical aerodynamic force showed a large force peak preceded by a small peak, during each wing stroke (forward and backward stroke). The back stroke produces a larger vertical force and a more distinct higher harmonic. These dynamics are similar between species, despite their different wing shapes. This suggests that wing shape does not strongly affect the characteristics of aerodynamic force production.

The wingbeat-average vertical aerodynamic forces showed a strong scaling with body mass (Figure 6D), as expected due to the differences in wing size between species (top row in Figure 6). For each studied species, we modelled aerodynamic forces, both at the species-specific wingbeat frequency and at the mean wingbeat frequency of all species (Figure 6B,D). For the simulations with species-specific wingbeat frequency, the hoverflies produced on average weight-support, whereas for the mean wingbeat frequency cases weight-support was not achieved (Figure 6D). Variation in wingbeat frequency thus appeared necessary for individual hoverflies to achieve weight support, although between species wingbeat frequencies do not correlate with body mass.

We continued to analyse the relative effect of variations in wing morphology and wingbeat-frequency on the aerodynamic force production, as quantified from CFD (Figure 7, Table 2). Here, all the tested morphology and kinematics parameters varied significantly with aerodynamic force magnitude, except for wingbeat-frequency and normalized second-moment-of-area.

First, we correlated the vertical forces computed using CFD with the product of second-moment-of-area and wingbeat-average angular speed squared (Figure 7A). According to our quasi-steady aerodynamic model, this should yield a linear correlation (Eqn 1: $F \sim S_2\,\overline{\omega}^2$), which was also the case as the allometric scaling factor of a_{all}=0.99 [0.97 – 1.01] (n=8) is not significantly different from linear (Table 2). The corresponding allometric scaling factor equals 103%, suggesting that the allometric adaptations that drive variations in $S_2\,\overline{\omega}^2$ fully explain variations in aerodynamic force production required for maintaining weight support across sizes. It also shows that our quasi-steady aerodynamic model predicts the effect of morphology and kinematics on aerodynamic force production well.

Separating this dependency of aerodynamic forces on $S_2\,\overline{\omega}^2$ into its primary components, second-moment-of-area and wingbeat frequency (Figure 7B-D), shows that allometric adaptations in second-moment-of-area and wingbeat frequency contribute 81% and 22% to maintaining weight support across sizes, respectively. Hereby, the aerodynamic forces do not scale significantly with wingbeat frequency (Figure 7B; Table 2), as was also the case for the equivalent correlation of wingbeat frequency with body mass (Figure 3F; Table 1). These combined results

confirm that adaptations in morphology drive variations in aerodynamic force production between hoverflies species of various sizes, although variations in wingbeat frequency cannot be ignored.

Further parting the effect of S_2 on aerodynamic force production into its components (Figure 7E-G) shows that allometric adaptations in wingspan R, mean chord $\bar{c}$ and normalized second-moment-of-area S_2^* contribute 55%, 19% and 5% to variations in aerodynamic force production across sizes, respectively (Figure 7H). Here, normalized second-moment-of-area did not significantly scale with vertical force production (Figure 7G; Table 2), as opposed to the significant scaling found in the corresponding analysis with body mass for the extended 28 species dataset (Figure 4D; Table 1).

The sum of the relative scaling factors of all metrics contributing to vertical force production (Eqn 2) equals 101% (Figure 7H), suggesting that these allometric adaptations combined fully explain variations in aerodynamic force production required for maintaining weight support across sizes. The here-identified effects of morphological traits on CFD-based forces are strikingly similar to those from the comparative analysis between morphology and body mass (Figure 4). This shows that our kinematics analysis based on eight species captures the major effects of wing morphology on aerodynamic force production, as expected based on the morphological analysis with the large sample size of 28 species.

Discussion

Allometric changes in wing morphology enables small hoverflies to maintain weight support during hovering

In this study, we investigated whether variation in body mass among hoverfly species is associated with changes in wingbeat kinematics or in wing morphology. Both components directly influence the aerodynamic forces produced by beating wings during flapping flight (Ellington, 1984b), and therefore could accommodate for maintaining weight support during evolutionary changes in size occurring throughout the diversification of hoverfly species. Comparing how wingbeat kinematics and wing morphology scale with body mass across hoverfly species, we showed that wing size and shape rather than wingbeat kinematics scale with body mass. This suggests that wing morphology might respond stronger than wingbeat kinematics to the constraints imposed for maintaining weight support during flight in hoverflies.

Changes in wing morphology associated with body mass variation are commonly observed in flying animals (Le Roy et al., 2019; Norberg, 2007; Rayner, 1988; Taylor and Thomas, 2014; Tercel et al., 2018), indicating that wing and body morphology evolve together as an integrated phenotype. Increasing size is usually not only associated with relatively larger wings, but also accompanied by changes in wing shape (Danforth, 1989; Outomuro et al., 2013). Teasing apart the changes in wing morphology resulting from constraints imposed by body mass from that of other selective pressures is however not straightforward. It is generally facilitated by comparing species with similar ecology, because this limits the effect of contrasted ecological pressures at play in different species (García and Sarmiento, 2012). Hoverfly species present a similar ecology in that all adults are specialised flower visitors (Klecka et al., 2018). Comparable selective regimes are thus likely acting on the evolution of flight performance and associated flight kinematics and morphology in adult hoverflies.

Shared ancestry can also affect the evolution of wing morphology and its effect should thus be controlled to understand how body mass may constrain the evolution of other traits (Blomberg et al., 2003). Among the 28 species studied here, variation in the measured morphological traits was significantly influenced by phylogenetic

history. In contrast, among the sub-set of eight species for which we studied flight kinematics, phylogenetic signal in flight traits was non-significant. This may suggest either a higher evolutionary lability in flight compared to morphological traits, or results from limited statistical power due to the small number of species with quantified flight data. Note that the lack of phylogenetic signal does not necessarily preclude an impact of phylogeny on the covariation between traits and body mass. As such, changes in wing morphology (and possibly in wingbeat kinematics) resulting from constraints imposed by body mass are confounded with the effect of shared ancestry. Our phylogenetically informed regressions of morphological and flight traits against body mass nonetheless allow disentangling such effects.

The large size variation among hoverfly species results from 90 million years of evolutionary diversification (Wong et al., 2023). While some taxa may have evolved larger body sizes than their ancestors, others may have undergone size reduction. Determining the exact trajectory of body size evolution in the species studied is beyond the scope of our study. Addressing the aerodynamic challenges of size reduction may not fully represent the evolutionary constraints acting on all hoverfly species. However, we chose to focus on the adaptation of the wing-based aerodynamic thrust-producing system in this context, as it provides a valuable framework for understanding the evolution of flight in small flying insects.

As size decreases, the wings become relatively less effective in producing the aerodynamic forces required for weight support (see Supplementary Text). The constraints imposed by weight support during hovering flight should then promote the evolution of disproportionately large wings, or an increased wingbeat frequency or amplitude in smaller hoverflies species. We found that none of wingbeat kinematic parameters significantly scaled with body mass but that wings indeed tended to be disproportionately larger in smaller species (i.e. negative allometry). Here, size-dependent adaptations in the primarily wing morphology parameter second-moment-of-areas (S_2; Eqn 1) almost fully explained the required adaptations for maintaining weight-support across sizes (a^*_{S2}=98%; Figure 4E). Parsing the second-moment-of-areas in its separate wing size and shape components shows that both the primary wing size wing shape metrics (wingspan *R* and dimensionless second-moment-of-areas S_2^*, respectively) exhibit significant negative allometric scaling (Figure 4B, D). These allometric adaptations in wing size and shape are predicted to contribute to maintaining weight-support across sizes for 71% and 5%, respectively (Figure 4F). Thus, changes in multiple aspects of the wing morphology may contribute to mitigating the negative effect of size reduction on flight ability, whereby wing shape effects are small but significant (Figure 5).

A negative allometry between wing size and body size has been found in other insect groups: for solitary bees this was found at both the interspecific and intraspecific level (Grula et al., 2021), and at the intraspecific level in rhinoceros beetles (Kawano, 1995). In contrast, disproportionately larger wing were found in larger species of dragonfly, suggesting positive allometry in these larger insects (May, 1981). This opposite allometric scaling of wing size in dragonflies and hoverflies may be the result of the use of contrasted mechanisms for producing aerodynamic forces, involving both morphological or kinematics variations, and contrasted flight modes (e.g., gliding flight in dragonflies).

The observed negative allometry in wing shape with mass was further emphasised in our geometric morphometrics analysis (Figures 5, S4 and S5). Indeed, in our phylogenetic Principal Component Analysis performed on superimposed wing shape coordinates, the primary axis PC1 explained a striking 69% of the

variations in wing shape, and was strongly correlated with normalised second-moment-of-area S_2^*. This PC1 shape variation depicts a shift in the spanwise distribution of wing area, from more proximally located in larger species to more distally located in smaller species (Figure 5). Interestingly, similar changes in wing shape associated with decreasing body size have been found among species of Hymenoptera (Danforth, 1989). An illustration of the most pronounced end of this pattern is the highly spatulated wing shape found in tiny wasp species (e.g. in the Mymaridae or Mymarommatidae families). This shows that although the relative contribution of allometric scaling of wing shape to maintaining weight support is relatively small (5%; Figure 4F), physical constraints associated with size reduction are strong enough to drive these adaptations. Evolutionary changes in the body size of hoverflies may thus have favoured wing shapes in smaller species that produce aerodynamic forces more effectively.

We continued to study how allometric variations in wing morphology and wingbeat kinematics affected aerodynamic force production across the studied range of hoverfly sizes (Figures 6 and 7). For this, we combined flight experiments on eight hoverfly species with both analytical quasi-steady aerodynamic modelling (Eqns 1,2) and numerical aerodynamics modelling (CFD). By combining these results, we first tested the validity of our quasi-steady aerodynamics model by correlating the wingbeat-average vertical forces estimated from CFD with the product of second-moment-of-area and wingbeat-average angular wing speed ($F \sim S_2\ \overline{\omega}^2$; Eqn 1; Figure 7A). The resulting linear correlation shows that our quasi-steady aerodynamic model captures the effect of wing morphology and kinematics on aerodynamic force production well. By separating the combined effect of variations in morphology and kinematics on aerodynamic force production into its components (Eqn 2), we confirm that adaptations in morphology drive the variations in aerodynamic force production between hoverfly species of different sizes. Here, wing size variations as expressed by wingspan have the largest effect on aerodynamic force production, but variations in wing shape and wingbeat frequency cannot be completely ignored (Figure 7C,G,H). In fact, the respective 5% and 22% contribution of wing shape and wingbeat frequency to variations in aerodynamic force production, need to be included in our model to maintain 100% weight support across the size range of our hovering hoverflies (Figure 7H).

Factors decoupling wingbeat kinematics from the influence of body mass

Our study revealed that wingbeat kinematics is relatively stable across hoverfly species, with none of the measured kinematics parameters significantly correlated with body mass (Figure 3; Table 1). Performing computational fluid dynamic simulations using the average wingbeat kinematics for all species, but incorporating differences in wing morphology, demonstrated that weight support was indeed achieved across species. Important however is that variation in wingbeat frequency – albeit uncorrelated with body mass – has proven crucial for correctly estimating the aerodynamic force necessary to achieve weight support (Figures 6D and 7C,D). Adjustments in wingbeat frequency thus appear to play a role in achieving weight support during hovering for individual hoverflies. The hovering hoverflies might thus primarily use wingbeat frequency to finely tune the vertical aerodynamic force required for weight support. Unlike birds and bats, flying insects cannot actively morph their wings to control aerodynamic force production (Harvey et al., 2022). As a result, flying insects rely purely on wingbeat kinematics changes to trim aerodynamic forces and torques during steady flight (Muijres et al., 2017), and to adjust these forces and torques during manoeuvring flight (Hedrick et al., 2009; Muijres et al., 2014). Our

CFD simulation results suggest that hovering hoverflies use relatively simple wingbeat frequency modulations to compensate for the continuous daily fluctuations in body mass, as a result of food and water intake and excretion.

The lack of covariation between in-flight wing movement and body mass goes against the prediction that wingbeat kinematics is more likely to be adjusted with varying body mass due to the greater flexibility of flight kinematics as compared to morphology. This finding is also surprising given that size variation is generally accompanied with changes in wingbeat kinematics in other flying animals (Norberg, 2007; Rayner, 1988; Riskin et al., 2010; Taylor and Thomas, 2014; Tercel et al., 2018). A previous study dissecting the flapping wing kinematics of miniaturised insects found an increased wing deviation in smaller species enabling higher wing velocity and hence aerodynamic force production (Lyu et al., 2019). Such a change in wing kinematics associated with decreasing size can be explained by the increased viscous drag constraint that tiny flying insects experience at low Reynolds numbers, requiring higher aerodynamic force generation. Here we did not find an increased wing deviation angle in smaller hoverfly species, most-likely because our study focusses on a too narrow range of sizes and consequently too similar Reynolds numbers. Our CFD analysis confirms this, as the effect of Reynold number aerodynamic force production was negligible.

While only a handful studies have examined the effect of body mass on detailed wingbeat kinematics in insects (such as wingbeat amplitudes and angle-of-attack Belyaev et al., 2014; Lyu et al., 2019; Meresman and Ribak, 2017), the scaling between body mass and wingbeat frequency has been frequently assessed (Bartholomew and Casey, 1978; Byrne et al., 1988; Casey et al., 1985; De Nadai et al., 2021; Dudley, 1990; Tercel et al., 2018). In theory, an increase in wingbeat frequency is expected in smaller insects because flapping wing-based aerodynamic force production decreases faster than body mass. As such, it is puzzling that the reduction in size among the studied hoverfly species is not associated with increased wingbeat frequency.

Interestingly, inconsistent results on the scaling between body mass and wingbeat frequency have been found among other groups of flying animals. Although predominantly negative (e.g. in butterflies (Dudley, 1990), in orchid bees (Darveau et al., 2005), in mosquitoes (De Nadai et al., 2021), and in a comparative study across insect orders (Tercel et al., 2018)), several studies found weak or no relationship between body mass and wingbeat frequency (e.g. in moths (Bartholomew and Casey, 1978), whiteflies (Byrne et al., 1988), bees (Duell et al., 2022; Grula et al., 2021)). Consistent with our findings, a study comparing the wingbeat kinematics during tethered flight among hoverfly species spanning a range of body mass similar to that investigated here found no significant effect of body mass on wingbeat kinematics (Belyaev et al., 2014).

A possible explanation to the heterogeneous trends found among insect groups is that the extent to which body mass constrains the evolution of wingbeat kinematics depends on species ecology. Adaptation to a particular ecological niche may drive the evolution of specialised flight abilities, promoting a specific wingbeat kinematics. Selective pressures exerted on these wingbeat kinematics may sometimes overcome the constraints imposed by weight support. In that case, relatively constant wingbeat kinematics would be maintained over a range of body mass, and changes in wing morphology alone are expected to adjust for weight support. Consistent with this hypothesis is the decoupling of wingbeat kinematics from body mass variation, which has been highlighted in species where hovering flight ability is crucial for food acquisition. These include bees (Duell et al., 2022; Grula et al., 2021), sphingid moth (Bartholomew and Casey, 1978), hummingbirds (Skandalis et al., 2017), and hoverflies

716 (Belyaev et al., 2014) as also in the present study. The absence of correlation between body mass and wingbeat
717 kinematics observed in hoverflies may thus be due to their highly specialised hovering flight abilities.
718 The selective pressures promoting the evolution of unique hovering flight abilities in hoverflies are not
719 precisely known but hovering steadily is likely advantageous for navigating between flowers when foraging for
720 nectar. Good hovering flight performance may also have been promoted because it increases mating
721 opportunities during the leck gathering of males (Downes, 1969; Gilbert, 1984; Heinrich and Pantle, 1975). Thus,
722 selection for increased foraging efficacy and/or mating opportunities may have maintained consistent wingbeat
723 kinematics across hoverfly species despite variation in body mass.
724 To further ascertain our findings, quantifying sexual dimorphism in hoverfly wingbeat kinematics would be a
725 relevant future research direction. This would clarify the role of mating behaviour on the evolution of hovering
726 flight performance. In this study, sexes could not be distinguished during our flight experiments, preventing us to
727 test whether male hoverflies exhibit better hovering performance. Furthermore, additional wingbeat kinematics
728 measurements in species from different habitats would help verifying the generality of our results in assessing
729 the possible effect of habitat. Contrasted environmental conditions (e.g., temperature, humidity, or altitude) can
730 affect flight performance (Altshuler and Dudley, 2003; Farnworth, 1972), and thus interfere with the scaling
731 between flight and morphology. Future research should also focus on how the variation in scaling highlighted
732 here influences peak locomotor performance. The effect of morphology on performance is generally most
733 pronounced when individuals are pushed to their limits (Losos et al., 2002). For instance, investigating how the
734 differential scaling between wing and body size affects peak thrust production during evasive flight manoeuvres
735 would be a relevant experiment for future study.
736
737 **CONCLUSION**
738 Altogether, our results suggest that the hovering flight abilities of hoverflies may stem from highly specialised
739 wingbeat kinematics that have been largely conserved throughout their diversification. In contrast, changes in
740 wing morphology have evolved with the aerodynamic constraints associated with evolutionary changes in size.
741 The existence of selective pressures maintaining stable wingbeat kinematics despite variation in body mass
742 implies that high hovering flight performance can only be achieved over a limited range of wingbeat kinematic
743 parameters, which remains to be ascertained.
744 Our study moreover highlights that unlike many other Diptera, hoverflies make use of a highly stereotyped
745 inclined stroke-plane wingbeat kinematics for hovering, where during the forward dorsal-ventral wing stroke the
746 wing moves not only from back to front but also downwards (Mou et al., 2011). This wingbeat kinematics pattern
747 may contribute to the specialised hovering abilities of hoverflies, as it is consistently observed among the eight
748 species studied here, with their stroke-plane pitch angle during hovering being approximately orientated at −30°.
749 Furthermore, despite significant changes in wing morphology and wingbeat frequency among the studied
750 species, the temporal dynamics of aerodynamic force production is strikingly similar between them (Figures 6C
751 and S6). This suggests that not only the wingbeat kinematics is conserved between species, but also the
752 underlying aerodynamics including the relative use of different unsteady aerodynamic mechanisms (Sane, 2003).
753 Thus, the apparent highly specialised flight style of hoverflies is maintained among several species with a large
754 range of body masses, and robust against variations in wing shape and wingbeat frequency.

List of symbols and abbreviations

a	scaling factor of a metric with body mass ($\sim m^a$)	[-]
a^*	relative scaling factor of a metric with body mass	[-]
α	wing angle-of-attack	[°]
$\bar{\alpha}$	mean angle-of-attack at mid-wing stroke	[°]
A_ϕ	wing stroke amplitude	[°]
A_θ	wing rotation amplitude	[°]
A_η	wing deviation amplitude	[°]
β_{body}	body pitch angle	[°]
$\beta_{stroke\text{-}plane}$	wing stroke plane angle relative to the horizontal	[°]
c	wing chord length	[cm]
$\bar{c}$	mean wing chord length	[cm]
C_F	lift force coefficient	[-]
$C_{F\alpha}$	angle-of-attack-specific lift force coefficient	[-]
f	wingbeat frequency	[Hz]
$\hat{f}$	mean wingbeat frequency over the full flight sequence	[Hz]
$\bar{f}$	mean wingbeat frequency across all species	[Hz]
F	aerodynamic lift force produced by a beating wing	[N]
F^*	aerodynamic lift force normalized by the wingbeat-average force	[-]
F/mg	weight-normalized aerodynamic lift force	[-]
g	gravitational acceleration	[m s^{-2}]
γ_{climb}	climb angle	[°]
J	advance ratio	[-]
m	body mass	[mg]
n	number of items in the dataset	[-]
ϕ	wing stroke angle	[°]
θ	wing rotation angle	[°]
η	wing deviation angle	[°]
$\dot{\phi}$	wing stroke rate	[° s^{-1}]
$\dot{\theta}$	wing rotation rate	[° s^{-1}]
$\dot{\eta}$	wing deviation rate	[° s^{-1}]
P	Probability	[-]
PCA	Principal Component Analysis	[-]
PC	Principal Component	[-]
r	regression parameter	[-]
r	position along the wingspan	[cm]
Re	Reynolds number	[-]
R	wingspan	[cm]
R^*	weight-normalised wingspan	[-]
$\bar{R}$	mean wingspan across all species	[cm]
ρ	air density	[kg m^{-3}]
S	wing surface area	[cm^2]
S_2	wing second-moment-of-area relative to the wing hinge	[cm^4]
S_2^*	non-dimensional second-moment-of-area	[-]

t	time	[sec]
$\mathbf{U}$	flight velocity vector in the world reference frame	[m s^{-1}]
U	flight speed	[m s^{-1}]
U_{hor}	horizontal flight velocity component	[m s^{-1}]
U_{ver}	vertical flight velocity component	[m s^{-1}]
ω	angular speed of a beating wing	[° s^{-1}]
$\bar{\omega}$	wingbeat-average angular wing speed	[° s^{-1}]
$\mathbf{X}=[x,y,z]$	coordinates in the world reference frame, with the z-axis vertical up	[m]

Acknowledgements

The authors would like to thank Ilam Bharathi for helpful discussions about insect flight aerodynamics, and Remco Pieters for his help in building and operating the experimental setup. We are grateful to the Naturalis Centre of Leiden for granting access to their Syrphidae collection, and in particular, to Pasquale Ciliberti for his help with handling collection specimens and taking photographs. We thank the three anonymous reviewers who greatly helped improving the first version of the manuscript.

Funding

This work was supported by an NWO Vidi research grant to F.T.M. (I/VI.Vidi.193.054). The study was also provided with computer and storage resources to T.E. by GENCI at IDRIS thanks to the grant 2023-A0142A14152 on the supercomputer Jean-Zay's CSL partition.

References

Adams DC, Otárola-Castillo E. 2013. geomorph: an R package for the collection and analysis of geometric morphometric shape data. *Methods in Ecology and Evolution* **4**:393–399.

Alexander RM. 2013. Principles of Animal Locomotion, Principles of Animal Locomotion. Princeton University Press. doi:10.1515/9781400849512

Altshuler DL, Dudley R. 2003. Kinematics of hovering hummingbird flight along simulated and natural elevational gradients. *Journal of Experimental Biology* **206**:3139–3147.

Bartholomew GA, Casey TM. 1978. Oxygen Consumption of Moths During Rest, Pre-Flight Warm-Up, and Flight in Relation to Body Size and Wing Morphology. *Journal of Experimental Biology* **76**:11–25. doi:10.1242/jeb.76.1.11

Batchelor GK. 1967. An Introduction to Fluid Dynamics. Cambridge University Press.

Bejan A, Marden JH. 2006. Unifying constructal theory for scale effects in running, swimming and flying. *Journal of Experimental Biology* **209**:238–248. doi:10.1242/jeb.01974

Belyaev OA, Chukanov VS, Farisenkov SE. 2014. Comparative characteristics of the wing apparatus and flight of Syrphid flies (Diptera: Syrphidae). *Moscow Univ BiolSci Bull* **69**:19–22. doi:10.3103/S0096392514010027

Blomberg SP, Garland Jr T, Ives AR. 2003. Testing for phylogenetic signal in comparative data: behavioral traits are more labile. *Evolution* **57**:717–745.

Bookstein FL. 1997. Morphometric tools for landmark data: geometry and biology. Cambridge University Press.

Byrne DN, Buchmann SL, Spangler HG. 1988. Relationship between wing loading, wingbeat frequency and body mass in homopterous insects. *Journal of Experimental Biology* **135**:9–23.

Casey TM, May ML, Morgan KR. 1985. Flight Energetics of Euglossine Bees in Relation to Morphology and Wing Stroke Frequency. *Journal of Experimental Biology* **116**:271–289. doi:10.1242/jeb.116.1.271

Clauset A, Erwin DH. 2008. The evolution and distribution of species body size. *Science* **321**:399–401.

Clemente CJ, Dick TJ. 2023. How scaling approaches can reveal fundamental principles in physiology and

biomechanics. *Journal of Experimental Biology* **226**:jeb245310.
Cloyed CS, Grady JM, Savage VM, Uyeda JC, Dell AI. 2021. The allometry of locomotion. *Ecology* **102**:e03369.
Cribellier A, Straw AD, Spitzen J, Pieters RP, van Leeuwen JL, Muijres FT. 2022. Diurnal and nocturnal mosquitoes escape looming threats using distinct flight strategies. *Current Biology* **32**:1232–1246.
Danforth BN. 1989. The evolution of hymenopteran wings: the importance of size. *Journal of Zoology* **218**:247–276.
Darveau C-A, Hochachka PW, Welch Jr KC, Roubik DW, Suarez RK. 2005. Allometric scaling of flight energetics in Panamanian orchid bees: a comparative phylogenetic approach. *Journal of Experimental Biology* **208**:3581–3591.
De Nadai B, Maletzke A, Corbi J, Batista G, Reiskind M. 2021. The impact of body size on Aedes [Stegomyia] aegypti wingbeat frequency: implications for mosquito identification. *Medical and Veterinary Entomology* **35**:617–624.
Dial KP, Greene E, Irschick DJ. 2008. Allometry of behavior. *Trends in ecology & evolution* **23**:394–401.
Dickinson MH, Muijres FT. 2016. The aerodynamics and control of free flight manoeuvres in Drosophila. *Philosophical Transactions of the Royal Society B: Biological Sciences* **371**:20150388.
Downes J. 1969. The swarming and mating flight of Diptera. *Annual review of entomology* **14**:271–298.
Dudley R. 1990. Biomechanics of flight in neotropical butterflies: morphometrics and kinematics. *Journal of Experimental Biology* **150**:37–53.
Duell ME, Klok CJ, Roubik DW, Harrison JF. 2022. Size-Dependent scaling of stingless bee flight metabolism reveals an energetic benefit to small body size. *Integrative and Comparative Biology* **62**:1429–1438.
Ellington C. 1984a. The aerodynamics of hovering insect flight. III. Kinematics. *Philosophical Transactions of the Royal Society of London B: Biological Sciences* **305**:41–78.
Ellington C. 1984b. The aerodynamics of hovering insect flight. IV. Aeorodynamic mechanisms. *Philosophical Transactions of the Royal Society of London B: Biological Sciences* **305**:79–113.
Ellington C. 1984c. The aerodynamics of insect flight. II. Morphological parameters. *Phil Trans R Soc Lond B* **305**:17–40.
Engels T, Schneider K, Reiss J, Farge M. 2021. A wavelet-adaptive method for multiscale simulation of turbulent flows in flying insects. *Commun Comput Phys* **30**:1118–1149.
Engels T, Truong H, Farge M, Kolomenskiy D, Schneider K. 2022. Computational aerodynamics of insect flight using volume penalization. *Comptes Rendus Mécanique* **350**:1–20. doi:10.5802/crmeca.129
Farnworth EG. 1972. Effects of ambient temperature, humidity, and age on wing-beat frequency of *Periplaneta* species. *Journal of Insect Physiology* **18**:827–839. doi:10.1016/0022-1910(72)90020-0
Fontaine EI, Zabala F, Dickinson MH, Burdick JW. 2009. Wing and body motion during flight initiation in Drosophila revealed by automated visual tracking. *Journal of Experimental Biology* **212**:1307–1323.
Fry SN, Sayaman R, Dickinson MH. 2003. The Aerodynamics of Free-Flight Maneuvers in Drosophila. *Science* **300**:495–498. doi:10.1126/science.1081944
García Z, Sarmiento CE. 2012. Relationship between body size and flying-related structures in Neotropical social wasps (Polistinae, Vespidae, Hymenoptera). *Zoomorphology* **131**:25–35. doi:10.1007/s00435-011-0142-z
Gilbert FS. 2015. Hoverflies (Naturalists' Handbooks). Pelagic Publishing.
Gilbert FS. 1984. Thermoregulation and the structure of swarms in Syrphus ribesii (Syrphidae). *Oikos* 249–255.
Gilbert FS. 1981. Foraging ecology of hoverflies: morphology of the mouthparts in relation to feeding on nectar and pollen in some common urban species. *Ecological Entomology* **6**:245–262. doi:10.1111/j.1365-2311.1981.tb00612.x
Gould SJ. 1966. Allometry and size in ontogeny and phylogeny. *Biological reviews* **41**:587–638.
Grula CC, Rinehart JP, Greenlee KJ, Bowsher JH. 2021. Body size allometry impacts flight-related morphology and metabolic rates in the solitary bee Megachile rotundata. *Journal of Insect Physiology* **133**:104275.
Gunz P, Mitteroecker P. 2013. Semilandmarks: a method for quantifying curves and surfaces. *Hystrix, the Italian Journal of Mammalogy* **24**:103–109.
Hanken J, Wake DB. 1993. Miniaturization of body size: organismal consequences and evolutionary significance. *Annual Review of Ecology and Systematics* **24**:501–519.
Hartley RI, Sturm P. 1995. Triangulation. Presented at the International Conference on Computer Analysis of Images and Patterns. Springer. pp. 190–197.

Harvey C, Baliga V, Wong J, Altshuler D, Inman D. 2022. Birds can transition between stable and unstable states via wing morphing. *Nature* **603**:648–653.
Hedrick TL, Cheng B, Deng X. 2009. Wingbeat time and the scaling of passive rotational damping in flapping flight. *Science* **324**:252–255.
Heinrich B, Pantle C. 1975. Thermoregulation in small flies (Syrphus sp.): basking and shivering. *Journal of Experimental Biology* **62**:599–610.
Hill AV. 1950. The dimensions of animals and their muscular dynamics. *Science Progress (1933-)* **38**:209–230.
Katzourakis A, Purvis A, Azmeh S, Rotheray G, Gilbert F. 2001. Macroevolution of hoverflies (Diptera: Syrphidae): the effect of using higher-level taxa in studies of biodiversity, and correlates of species richness. *Journal of Evolutionary Biology* **14**:219–227.
Kawano K. 1995. Horn and wing allometry and male dimorphism in giant rhinoceros beetles (Coleoptera: Scarabaeidae) of tropical Asia and America. *Annals of the Entomological Society of America* **88**:92–99.
Klecka J, Hadrava J, Biella P, Akter A. 2018. Flower visitation by hoverflies (Diptera: Syrphidae) in a temperate plant-pollinator network. *PeerJ* **6**:e6025.
Labonte D, Clemente CJ, Dittrich A, Kuo C-Y, Crosby AJ, Irschick DJ, Federle W. 2016. Extreme positive allometry of animal adhesive pads and the size limits of adhesion-based climbing. *Proceedings of the National Academy of Sciences* **113**:1297–1302. doi:10.1073/pnas.1519459113
Le Roy C, Debat V, Llaurens V. 2019. Adaptive evolution of butterfly wing shape: from morphology to behaviour. *Biological Reviews* **94**:1261–1281.
Losos JB, Creer DA, Schulte Ii JA. 2002. Cautionary comments on the measurement of maximum locomotor capabilities. *Journal of Zoology* **258**:57–61.
Lyu YZ, Zhu HJ, Sun M. 2019. Flapping-mode changes and aerodynamic mechanisms in miniature insects. *Physical Review E* **99**:012419.
May M. 1981. Allometric analysis of body and wing dimensions of male Anisoptera. *Odonatologica* **10**:279–291.
Meresman Y, Ribak G. 2017. Allometry of wing twist and camber in a flower chafer during free flight: How do wing deformations scale with body size? *Royal Society Open Science* **4**:171152.
Mou XL, Liu YP, Sun M. 2011. Wing motion measurement and aerodynamics of hovering true hoverflies. *Journal of Experimental Biology* **214**:2832–2844.
Muijres FT, Elzinga MJ, Melis JM, Dickinson MH. 2014. Flies evade looming targets by executing rapid visually directed banked turns. *Science* **344**:172–177.
Muijres FT, Iwasaki NA, Elzinga MJ, Melis JM, Dickinson MH. 2017. Flies compensate for unilateral wing damage through modular adjustments of wing and body kinematics. *Interface Focus* **7**:20160103.
Nath T, Mathis A, Chen AC, Patel A, Bethge M, Mathis MW. 2019. Using DeepLabCut for 3D markerless pose estimation across species and behaviors. *Nat Protoc* **14**:2152–2176. doi:10.1038/s41596-019-0176-0
Norberg U. 2007. Flight and scaling of flyers in nature. *Flow phenomena in nature* **1**:120–154.
Norberg UM. 2012. Vertebrate flight: mechanics, physiology, morphology, ecology and evolution. Springer Science & Business Media.
Outomuro D, Adams DC, Johansson F. 2013. Wing shape allometry and aerodynamics in calopterygid damselflies: a comparative approach. *BMC evolutionary biology* **13**:118.
Peattie AM, Full RJ. 2007. Phylogenetic analysis of the scaling of wet and dry biological fibrillar adhesives. *Proceedings of the National Academy of Sciences* **104**:18595–18600. doi:10.1073/pnas.0707591104
Pélabon C, Firmat C, Bolstad GH, Voje KL, Houle D, Cassara J, Rouzic AL, Hansen TF. 2014. Evolution of morphological allometry. *Annals of the New York Academy of Sciences* **1320**:58–75.
Ratnasingham S, Hebert PD. 2007. BOLD: The Barcode of Life Data System (http://www. barcodinglife. org). *Molecular ecology notes* **7**:355–364.
Rayner JM. 1988. Form and function in avian flightCurrent Ornithology. Springer. pp. 1–66.
Revell LJ. 2012. phytools: an R package for phylogenetic comparative biology (and other things). *Methods in Ecology and Evolution* **3**:217–223.
Riskin DK, Iriarte-Díaz J, Middleton KM, Breuer KS, Swartz SM. 2010. The effect of body size on the wing movements of pteropodid bats, with insights into thrust and lift production. *Journal of Experimental Biology* **213**:4110–4122.
Rohlf FJ. 2015. The tps series of software. *Hystrix* **26**:1–4.

Rohlf FJ, Slice D. 1990. Extensions of the Procrustes method for the optimal superimposition of landmarks. *Systematic Biology* **39**:40–59.

Sane SP. 2003. The aerodynamics of insect flight. *Journal of Experimental Biology* **206**:4191–4208.

Schmidt-Nielsen K. 1975. Scaling in biology: the consequences of size. *Journal of Experimental Zoology* **194**:287–307.

Skandalis DA, Segre PS, Bahlman JW, Groom DJ, Welch Jr KC, Witt CC, McGuire JA, Dudley R, Lentink D, Altshuler DL. 2017. The biomechanical origin of extreme wing allometry in hummingbirds. *Nature communications* **8**:1047.

Symonds MRE, Blomberg SP. 2014. A Primer on Phylogenetic Generalised Least Squares In: Garamszegi LZ, editor. Modern Phylogenetic Comparative Methods and Their Application in Evolutionary Biology: Concepts and Practice. Berlin, Heidelberg: Springer. pp. 105–130. doi:10.1007/978-3-662-43550-2_5

Taylor GK, Thomas ALR. 2014. Evolutionary Biomechanics: Selection, Phylogeny, and Constraint. Oxford University Press.

Tercel MP, Veronesi F, Pope TW. 2018. Phylogenetic clustering of wingbeat frequency and flight-associated morphometrics across insect orders. *Physiological Entomology* **43**:149–157.

Theriault DH, Fuller NW, Jackson BE, Bluhm E, Evangelista D, Wu Z, Betke M, Hedrick TL. 2014. A protocol and calibration method for accurate multi-camera field videography. *Journal of Experimental Biology* jeb.100529.

Tian F-B, Luo H, Song J, Lu X-Y. 2013. Force production and asymmetric deformation of a flexible flapping wing in forward flight. *Journal of Fluids and Structures* **36**:149–161. doi:10.1016/j.jfluidstructs.2012.07.006

Walker SM, Thomas AL, Taylor GK. 2010. Deformable wing kinematics in free-flying hoverflies. *Journal of the Royal Society Interface* **7**:131–142.

Weis-Fogh T. 1973. Quick estimates of flight fitness in hovering animals, including novel mechanisms for lift production. *Journal of Experimental Biology* **59**:169–230.

Wong DTL, Norman H, Creedy TJ, Jordaens K, Moran KM, Young A, Mengual X, Skevington JH, Vogler AP. 2023. The phylogeny and evolutionary ecology of hoverflies (Diptera: Syrphidae) inferred from mitochondrial genomes. *Molecular Phylogenetics and Evolution* 107759.

Figures

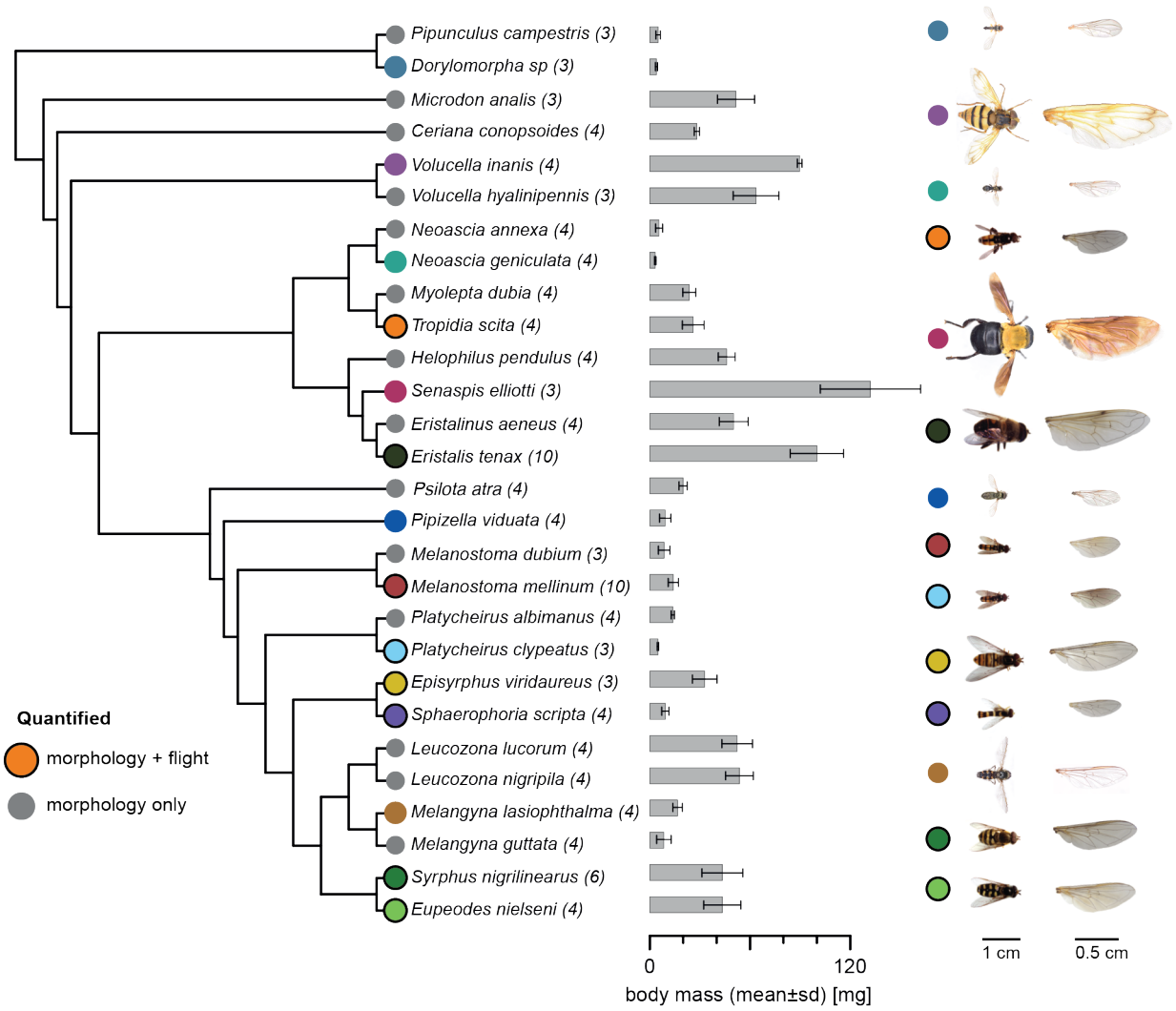

Figure 1. The studied hoverfly species shown with their phylogenetic relationships. Sample size as number of individuals for each species is in parentheses. Species marked with coloured circles are displayed on the right, and coloured circles with black outlines are of species for which both morphology and flight kinematics were quantified. Body mass is presented as mean values and standard deviation. Phylogeny was obtained from Wong et al. (2023).

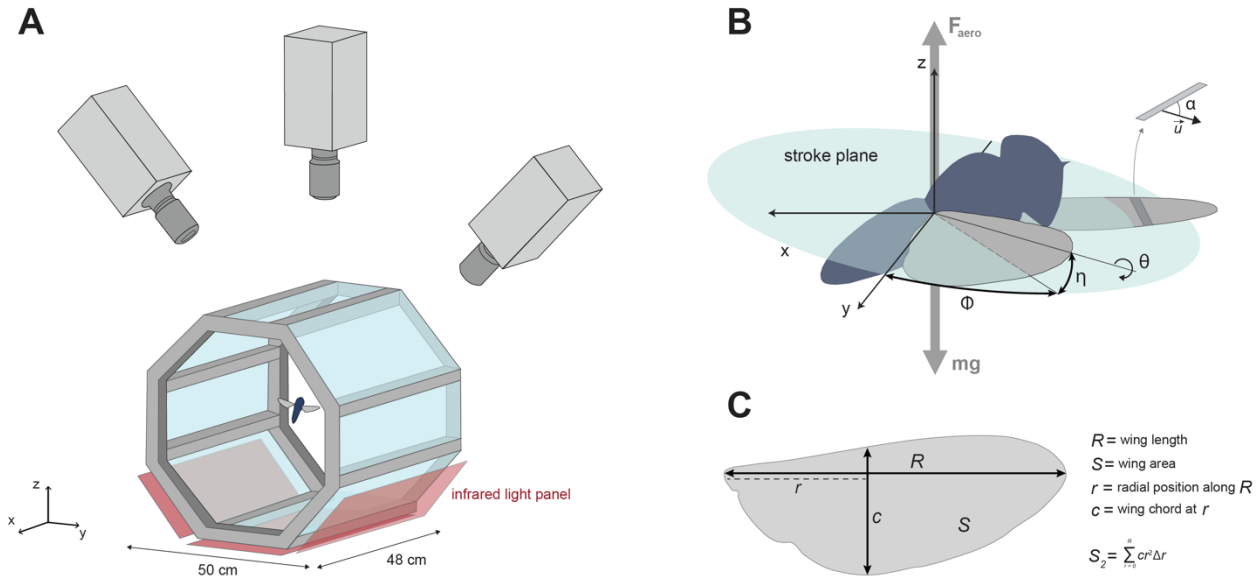

Figure 2. Quantifying the in-flight wingbeat kinematics and wing morphology of hoverflies. (A) Hoverflies were released in an octagon-shaped flight arena. We recorded stereoscopic high-speed videos of the flying hoverflies using three synchronised high-speed video cameras; from the videos we reconstructed the three-dimensional body and wingbeat kinematics. Infrared light panels positioned as the bottom of the arena enabled high contrast between the flying insect and the background. (B) Conventional wing angles were measured at each time step (t=0.0004 s) in the body reference frame. ϕ, wing stroke angle within the stroke plane; η, wing deviation angle out of the stroke plane; θ, wing rotation angle along the spanwise axis; $\vec{u}$, air velocity vector relative to the wing; α, angle-of-attack of the wing. (C) Wing morphological parameters including their definitions: wingspan R, wing surface area S, radial position along the span r, local wing chord c at distance r, and the second-moment-of-area S_2.

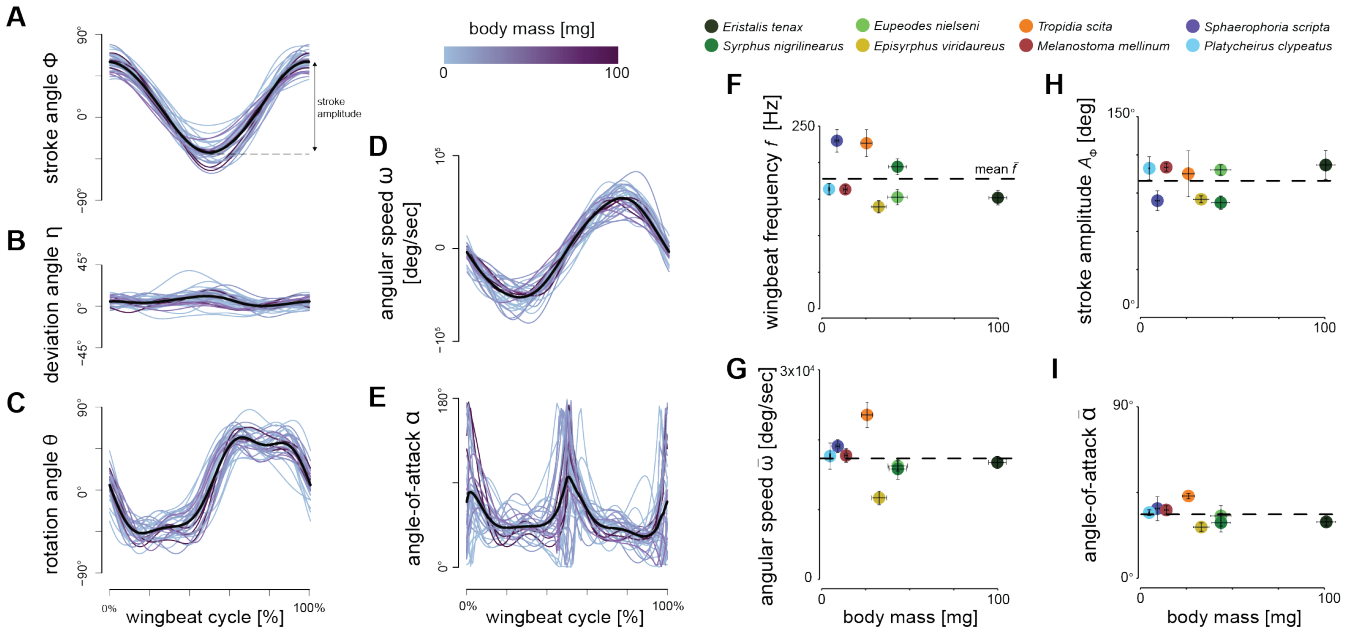

Figure 3. Wingbeat kinematics during hovering flight of the eight studied hoverfly species. (A-E) Temporal dynamics of the wingbeat kinematics throughout the wingbeat cycle of all digitised wingbeats. Separate wingbeats are colour coded by body mass (see legend on top), and the black lines show the average wingbeat kinematics for all wingbeats combined. (A-C) Temporal dynamics of the three conventional wingbeat kinematics angle (stroke, deviation, and rotation angle, respectively; see Figure 2 for definitions). (D-E) Angular speed and angle-of-attack of the wings throughout the wingbeat cycle, derived from wing stroke, deviation and rotation angles. (F-I) Derived wingbeat-average wingbeat kinematics parameters for each studied species versus the body mass of that species. The kinematics parameters are wing stroke amplitude A_ϕ, wingbeat frequency f, wingbeat-average angular wing speed $\overline{\omega}$, and mean angle-of-attack at mid wing stroke $\overline{\alpha}$, respectively. Each data point shows mean ± standard error per species, and is colour-coded according to the legend on the top. None of the wingbeat-average wingbeat kinematic parameters were significantly associated with body mass (Table 1). Horizontal dashed lines show the mean parameter values, as expected under kinematic similarity.

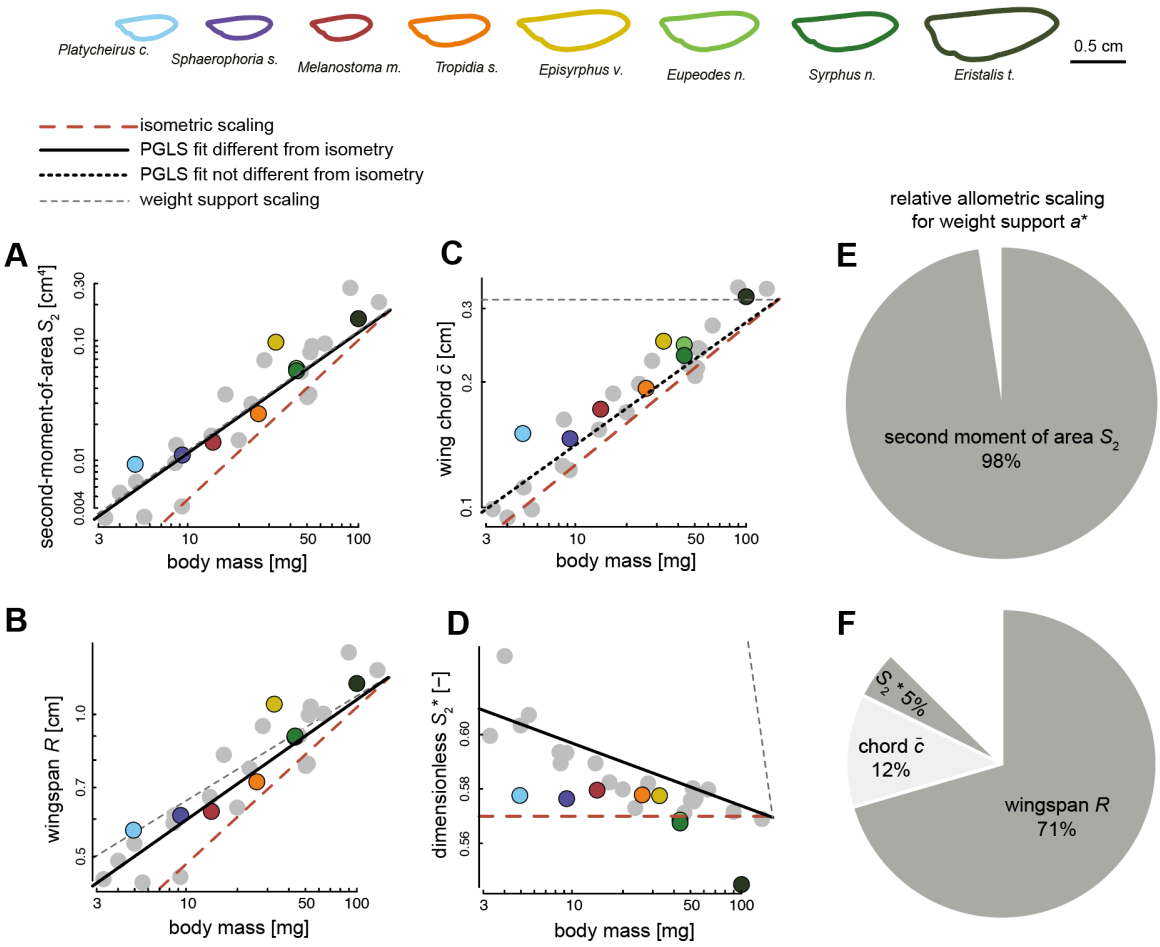

Figure 4. The scaling of wing morphology with body mass for all 28 studied hoverfly species (A-D), and how allometric scaling of wing morphology contributes to maintaining weight support across the hoverfly size range (E,F). (A-D) body mass (abscissa) versus on the ordinate the second-moment-of-area S_2, wingspan R, mean chord $\bar{c}$, and normalized second-moment-of-area S_2^*, respectively. Each data point shows a species average value, where data points of species for which flight was studied are colour-coded (see top row), and species with only quantified morphology are shown in grey (see the corresponding individual-specific data in Figure S3). The black, red and grey trendlines show the best fitting line from a PGLS regression, isometric scaling, and the expected scaling for metric-specific maintenance of weight support, respectively (see legend above A). All fitted PGLS regression slopes, except for wing chord, are significantly lower than expected under isometry, suggesting negative allometric scaling of wing size and shape with respect to body mass (see also Table 1). (E,F) The relative contributions of different wing morphology metrics to maintaining weight-support across the studied range of hoverfly sizes, expressed by the relative allometric scaling factor a^*. (E) the relative allometric scaling factor for the second-moment-of-area S_2, and (F) the relative allometric scaling factor for the separate morphological components of S_2: wingspan R, mean chord $\bar{c}$, and normalized second-moment-of-area S_2^*.

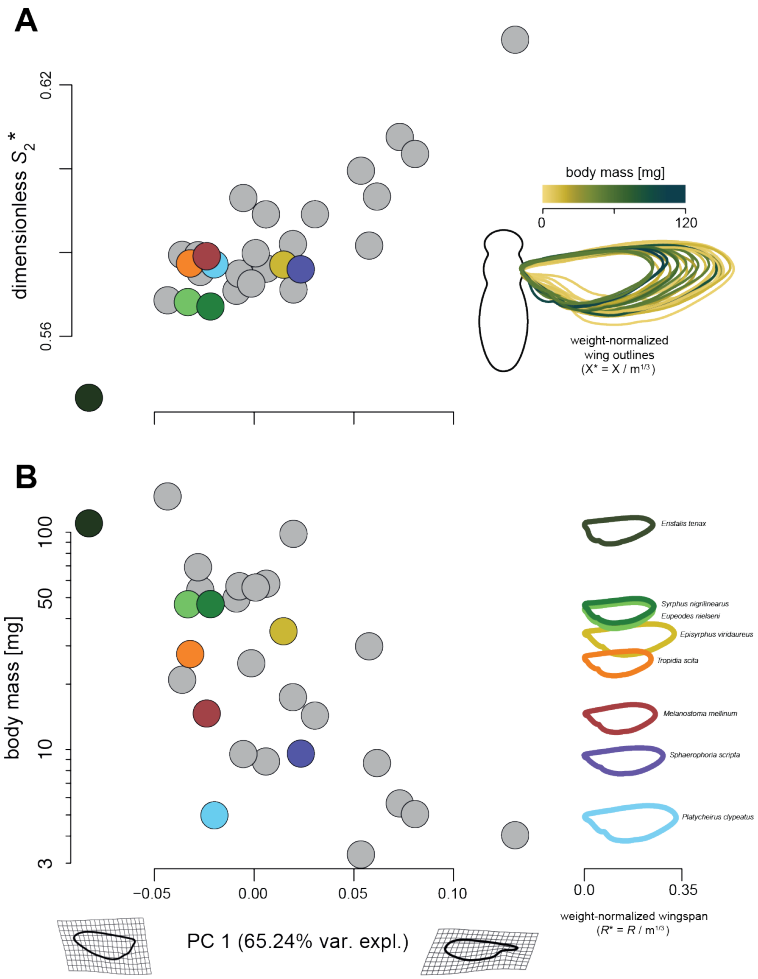

Figure 5. Changes in wing shape and size associated with body mass variation. Each data point shows a species-average value (see the individual-specific data in Figure S5), and are colour-coded for species of which both flight and morphology were studied (see right column of B), and in grey for species with only morphology quantified. (A) Normalised second-moment-of-area (S_2^*) versus the primary Principal Component (PC1) of the phylogenetic Principal Component Analysis (phyloPCA) performed on the mean wing shape coordinates of all 28 studied hoverfly species. On the right, we show the 28 wing outlines colour-coded and normalised with body mass (with coordinates $X^* = X/m^{1/3}$). (B) body mass (m) versus PC1 (left), and mass-normalised wing outlines versus body mass for the eight species used in our flight experiments (right). The left and right gritted wing shapes on the PC1 axis show the theoretical wing shapes at maximum and minimum value of PC1. PC1 explains 65.24% of the variations in wing shape (see also Figures S4 and S5). (A-B) The combined results show that in larger species, wing surface area was located more proximally (lower PC1 and S^*_2 values) than in smaller species, in which wing area tend to be located more distally (higher PC1 and S^*_2 values). Combined with the changes in wing shape (left), weight-normalised wingspan (R^*) and mean chord ($\bar{c}$) tend to be larger in smaller species (right).

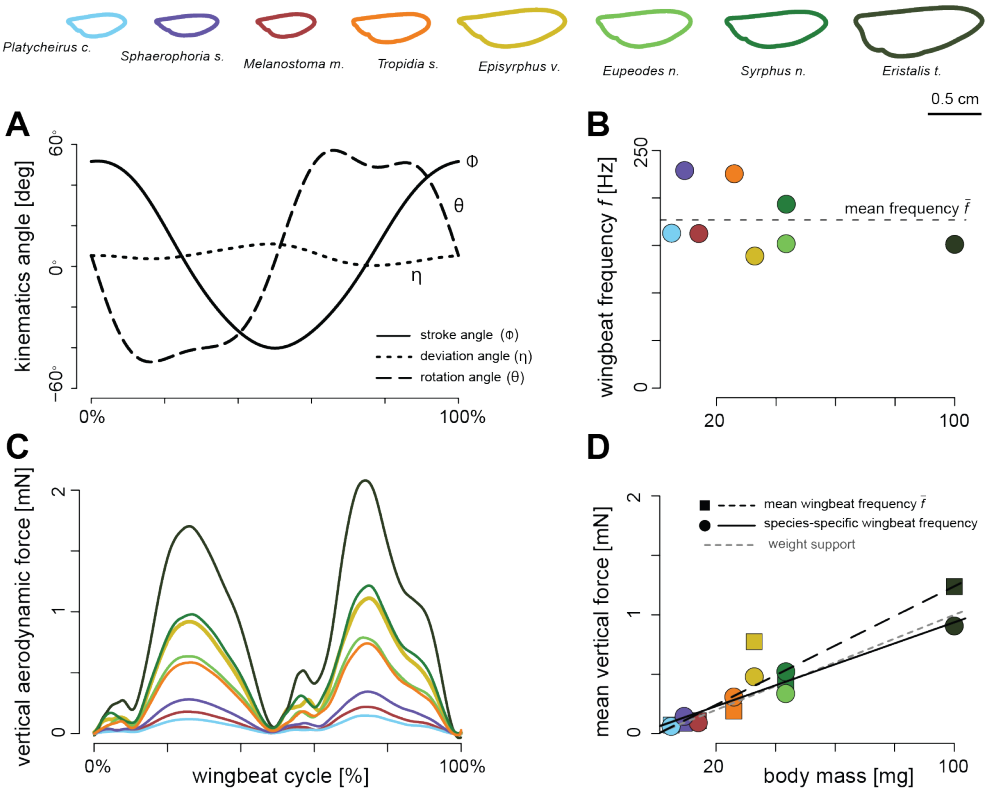

Figure 6. Aerodynamic forces produced by hovering hoverflies, as estimated using Computational Fluid Dynamic (CFD) simulations. (A-B) For our simulations, we used the species-specific wing shapes and sizes (top row), but average wingbeat kinematics and frequency ($\bar{f}$) across all eight studied hoverfly species (A,B). (C) The resulting temporal dynamic of vertical forces throughout the wingbeat cycle, coloured by species (see legend on top). (D) The wingbeat-average vertical force versus body mass, for all simulated hoverfly species operating at the average wingbeat frequency for all species $\bar{f}$ (square data points and dashed trend line), and forces scaled to the species-specific wingbeat frequency f (round data points in B and D, and solid trend line). The trendline for weight support ($F=mg$) is shown with a grey dashed line. With the species-specific wingbeat frequency f (solid trend line and circles in B and D) hoverflies are closer to producing weight support than for the simulations at the average wingbeat frequency $\bar{f}$ (dashed lines in B and D).

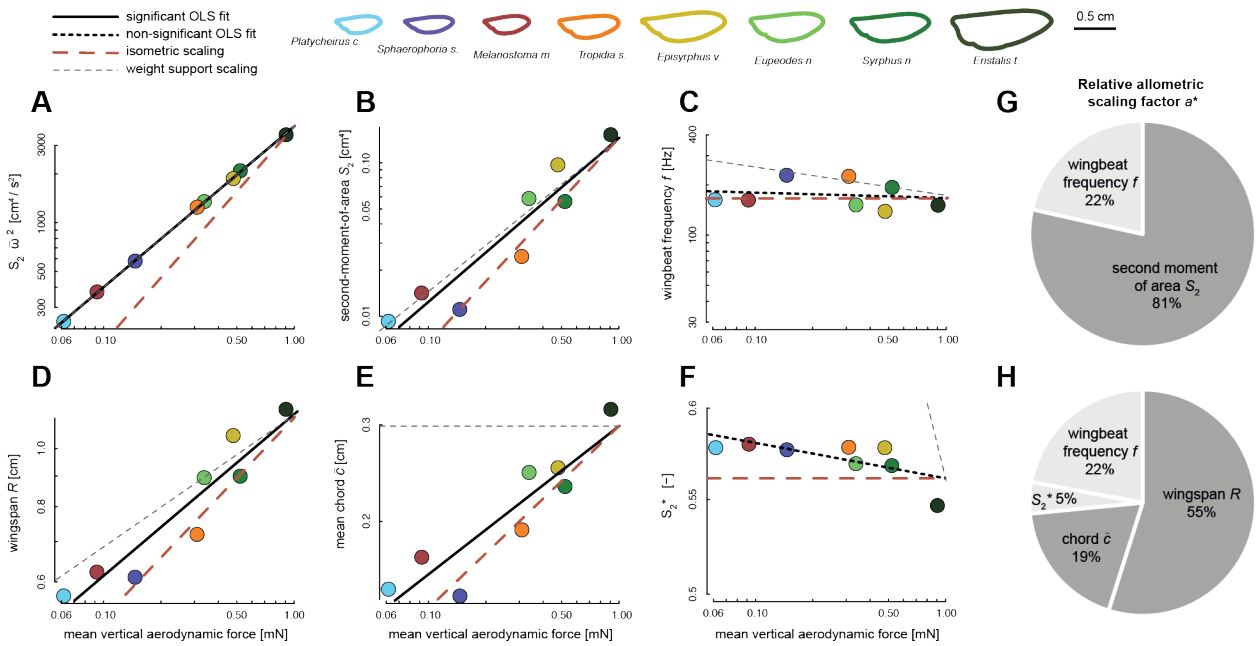

Figure 7. The relative contribution of allometric variations in wing morphology and wingbeat kinematics to CFD-derived vertical aerodynamic force production, and how this contributes to maintaining in-hovering weight-support across the sampled range of hoverfly sizes. (A-C, D-F) Wingbeat-average vertical force at species-specific wingbeat frequency *f* (abscissa) *vs.* on the ordinate various wing morphology and kinematics traits. In each panel, data points are results for different species, colour-coded according to the legend on the top. The solid and dashed black lines show the significant and non-significant OLS regression fits, respectively. The dashed red and grey lines show the expected slopes for scaling under morphological and kinematic similarity and for 100% metric-specific weight-support, respectively. (G,H) The relative contributions of allometric variations in wing morphology and kinematics to maintaining weight-support across the studied range of hoverfly sizes, expressed by the relative allometric scaling factor *a** (Eqn 3). Contributions based on significant and non-significant OLS regressions are shown in dark and light grey, respectively. (A) The wingbeat-average vertical force scales linearly with the product of second-moment-of-area and wingbeat-average angular speed squared (Eqn 1: $F \sim S_2\ \overline{\omega}^2$), resulting in weight-support across all sizes. (B-C) Separating this product into its main components (B and C, respectively) shows that the second-moment-of-area and wingbeat frequency contribute 81% and 22% to maintaining weight support across sizes, respectively (D). (E-H) Parting the contribution of second-moment-of-area into its components (D-F) shows that allometric variations in wingspan, mean chord and nondimensional second-moment-of-area contribute 55%, 19% and 5% to maintaining weight support across sizes, respectively (H).

Tables

Table 1. Results of phylogenetic general least square (PGLS) regressions of the log10-transformed morphological and wingbeat kinematic parameters from the aerodynamic model (Eqns 1,2) relative to log10-transformed body mass. Estimated scaling factors with 95% confidence intervals that exclude the scaling factor for isometry are indicated in bold and with a star, suggesting allometric scaling of that metric (see last column). The preceding two columns show the scaling factor for geometric or kinematic similarity, and the scaling factor for maintaining weight support across sizes via allometric changes of the specific parameter, assuming all other parameters scale under geometric and kinematic similarity.

	n	P	R^2 (%)	Intercept	Scaling factor estimate [95% C.I.]	Scaling factor for similarity	Scaling factor for single-metric weight support	Allometry
Wing morphology								
Second-moment-of-area S_2	28	**<0.001**	85.94	-2.949	**1.008 [0.767 – 1.250] ***	4/3 = 1.33	1	**negative**
Wingspan R	28	**<0.001**	83.67	-0.479	**0.255 [0.192 – 0.317] ***	1/3 = 0.33	2/9 = 0.22	**negative**
Wing chord $\bar{c}$	28	**<0.001**	87.77	-1.145	0.294 [0.229 – 0.359]	1/3 = 0.33	0	isometry
Normalized second-moment-of-area S_2*	28	**<0.001**	33.81	-0.206	**-0.017 [-0.025 – -0.009] ***	0	-1/3 = -0.33	**negative**
Wingbeat kinematics								
Wingbeat frequency f	8	0.427	0.09	2.343	-0.084 [-0.161 – 0.063]	0	-1/6 = -0.17	-
Stroke amplitude A_ϕ	8	0.785	0.01	2.041	-0.017 [-0.134 – 0.101]	0	-1/6 = -0.17	-
Wing angular speed $\bar{\omega}$	8	0.225	0	10.161	-0.101 [-0.249 – 0.046]	0	-1/6 = -0.17	-
Angle-of-attack $\bar{\alpha}$	8	0.105	0.22	3.947	-0.085 [-0.174 – 0.002]	0	-1/3 = -0.33	-

Table 2. Results of ordinary least square (OLS) regression between the log10-transformed vertical aerodynamic force estimated from CFD and log10-transformed morphological and kinematics parameters, for all eight hoverfly species studied using CFD. OLS regressions for metrics that scale significantly with aerodynamic force magnitude are indicated with a star, and have P-values in bold (**P<0.05**). For each tested parameter, we estimated its relative contribution to maintaining weight support across sizes using the relative allometric scaling factor a* (Eqn 3), based on the estimated scaling factor, the scaling factor for geometric or kinematic similarity, and the expected scaling for maintaining metric-specific weight support.

	n	P	R^2 (%)	Intercept	Scaling factor estimate [95% C.I.]	Scaling factor for similarity	Scaling factor for metric-specific weight support	relative allometric scaling factor *a* *
Wing morphology & kinematics								
$S_2 \cdot \omega^{-2}$	8	**<0.001***	99.93	3.593	0.989 [0.974 – 1.005]	4/3 = 1.33	1	103%
Second moment of area S_2	8	**<0.001***	87.78	-0.844	1.063 [0.667 – 1.461]	4/3 = 1.33	1	81%
Wingbeat frequency f	8	0.667	3.28	2.218	-0.037 [-0.238 – 0.164]	0	-1/6 = -0.17	22%
Wing morphology components								
Wingspan R	8	**<0.001***	88.38	0.058	0.272 [0.173 – 0.371]	1/3 = 0.33	2/9 = 0.22	55%
Wing chord $\bar{c}$	8	**0,001***	82.86	-0.525	0.271 [0.147 – 0.394]	1/3 = 0.33	0	19%
Normalized second moment of area S_2 *	8	0.055	48.32	-0.252	-0.015 [-0.031 – 0.000]	0	-1/3 = -0.33	5%

Supplementary material

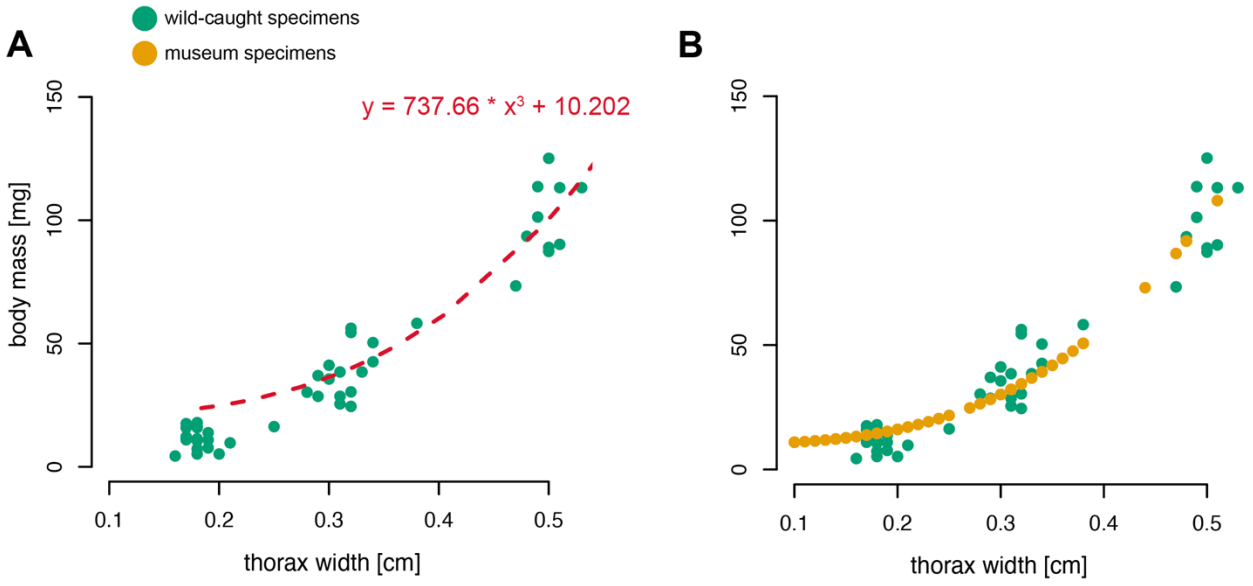

Figure S1. The body mass of museum specimens was approximated using the relationship between thorax width and the fresh mass in wild caught specimens. (**A**) A cubic polynomial regression model was fitted to the data from wild caught specimens. (**B**) The equation of the fitted model was used to estimated body mass from thorax width in museum specimens.

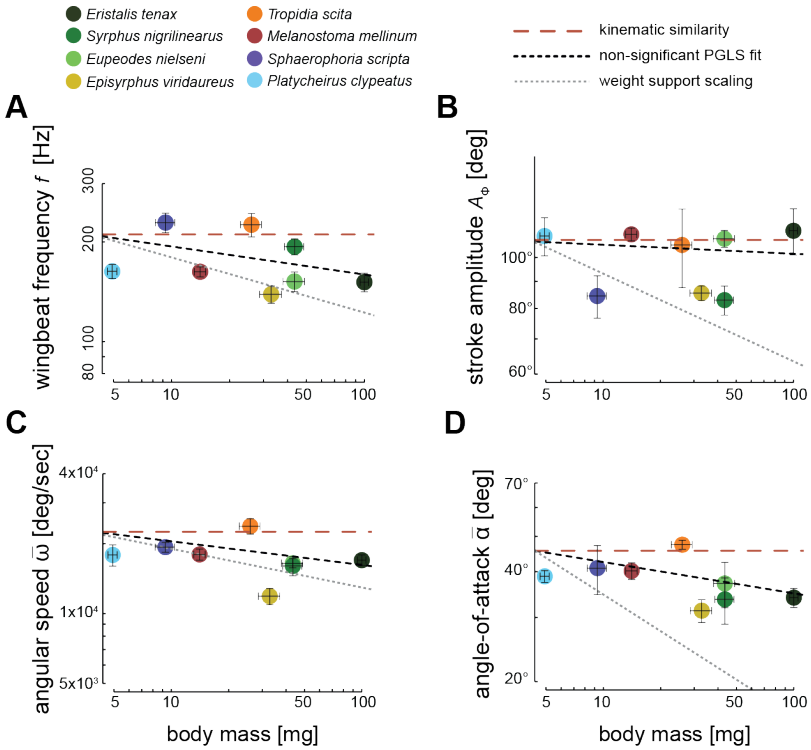

Figure S2. Derived wingbeat-average wing kinematics parameters for each studied species versus the body mass of that species. The kinematics parameters are (A) wingbeat frequency f, (B) wing stroke amplitude A_ϕ (C) wingbeat-average angular wing speed $\overline{\omega}$, and (D) mean angle-of-attack at mid wing stroke $\overline{\alpha}$, respectively. Each data point shows mean ± standard error per species. None of the wingbeat kinematic parameters were significantly associated with body mass, as shown by the non-significant dashed black trend lines from PGLS regressions. The corresponding scaling based on kinematic similarity is shown with red dashed lines, and the expected scaling for maintaining weight support across sizes, when assuming that all other parameters scale under kinematic similarity are shown in dotted grey lines (see Table 1 for details).

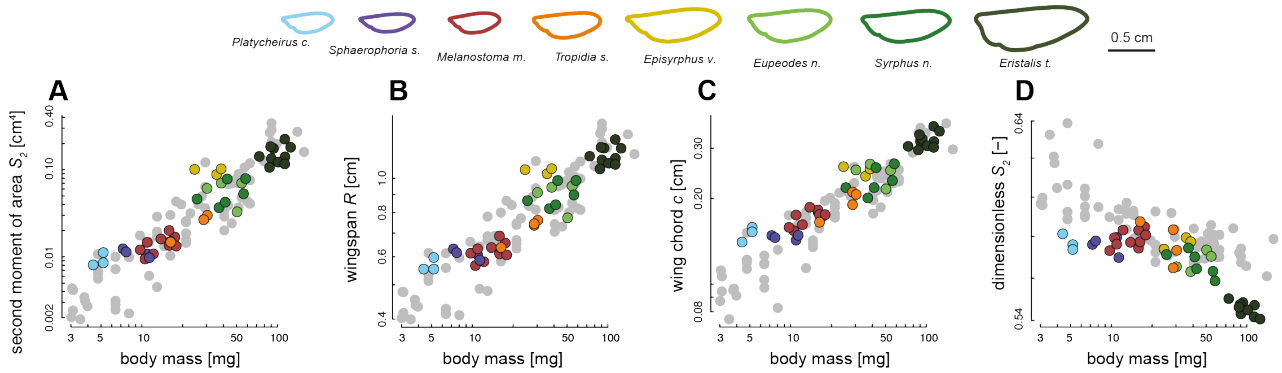

Figure S3. Wing morphology parameters versus body mass for all studied specimens. (A-D) body mass (abscissa) versus on the ordinate the second-moment-of-area S_2, wingspan R, mean chord $\bar{c}$, and normalized second-moment-of-area S_2^*, respectively. Each circle shows data for a different individual. Species for which both flight and morphology were studied are colour-coded (see top row), whereas species with only quantified morphology are shown in grey.

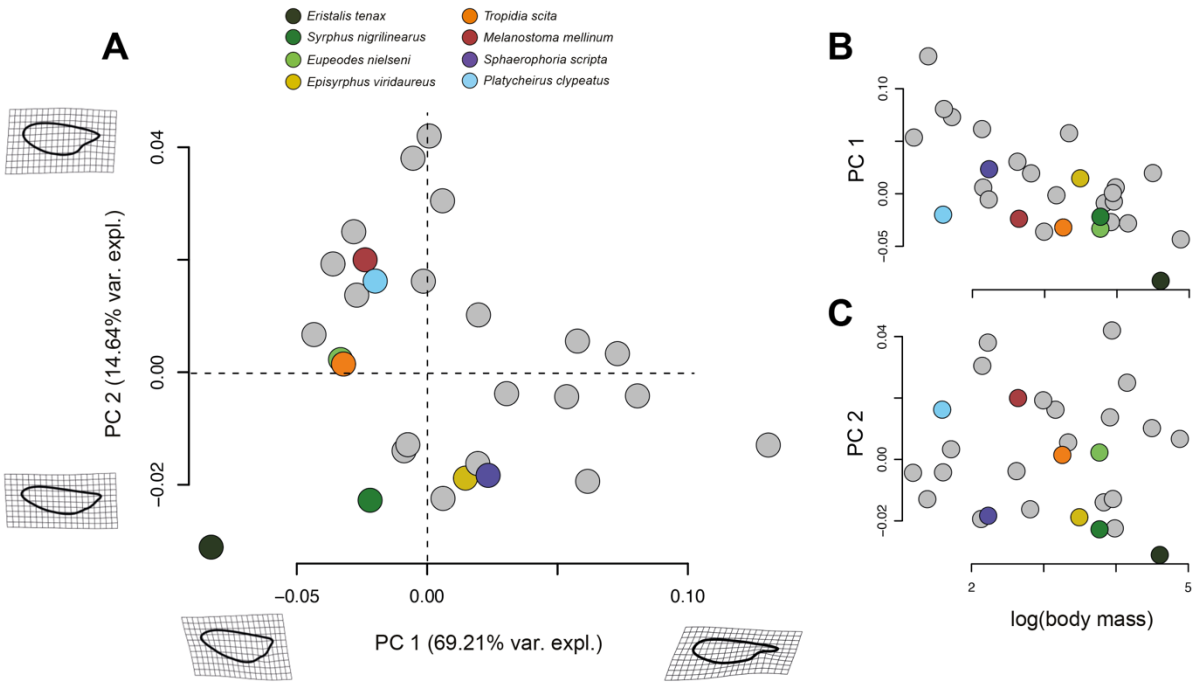

Figure S4. Result of geometric morphometrics analysis on the wing outlines of 28 hoverfly species. Species for which both flight and morphology were studied are colour-coded (see top row), whereas species with only quantified morphology are shown in grey. (A) The first two principal components (PC1 and PC2) from the phylogenetic principal component analysis (phyloPCA) on the geometric morphometrics data, along with the associated shape changes and the percentage of variation explained by these principal components. Shown wing shapes represent the extreme values associated with each PC axis. (B) PC1 and PC2 (first and second row, respectively) plotted against body mass, highlighting that the change in wing shape carried on PC1 is associated with variations in body mass.

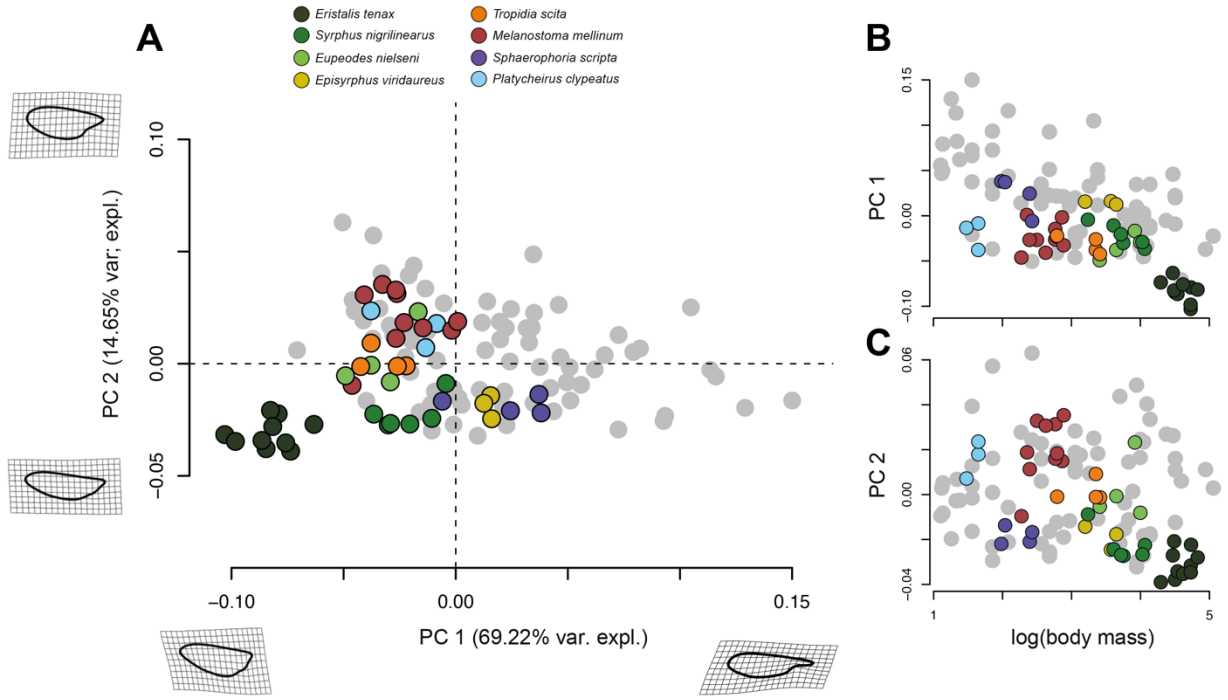

Figure S5. Result of geometric morphometrics analysis on the wing outlines of 28 hoverfly species. Each data point shows a different individual value. Species for which both flight and morphology were studied are colour-coded (see top row), whereas species with only quantified morphology are shown in grey. (A) The two first principal components (PC1 and PC2) of the phylogenetic Principal Component Analysis (phyloPCA), together with the associated shape changes and percentage of the variation explained by the principal components. Shown wing shapes represent the extreme values associated with each PC axis. (B) PC1 and PC2 (first and second row, respectively) plotted against body mass, highlighting that the change in wing shape carried on PC1 is associated with variations in body mass.

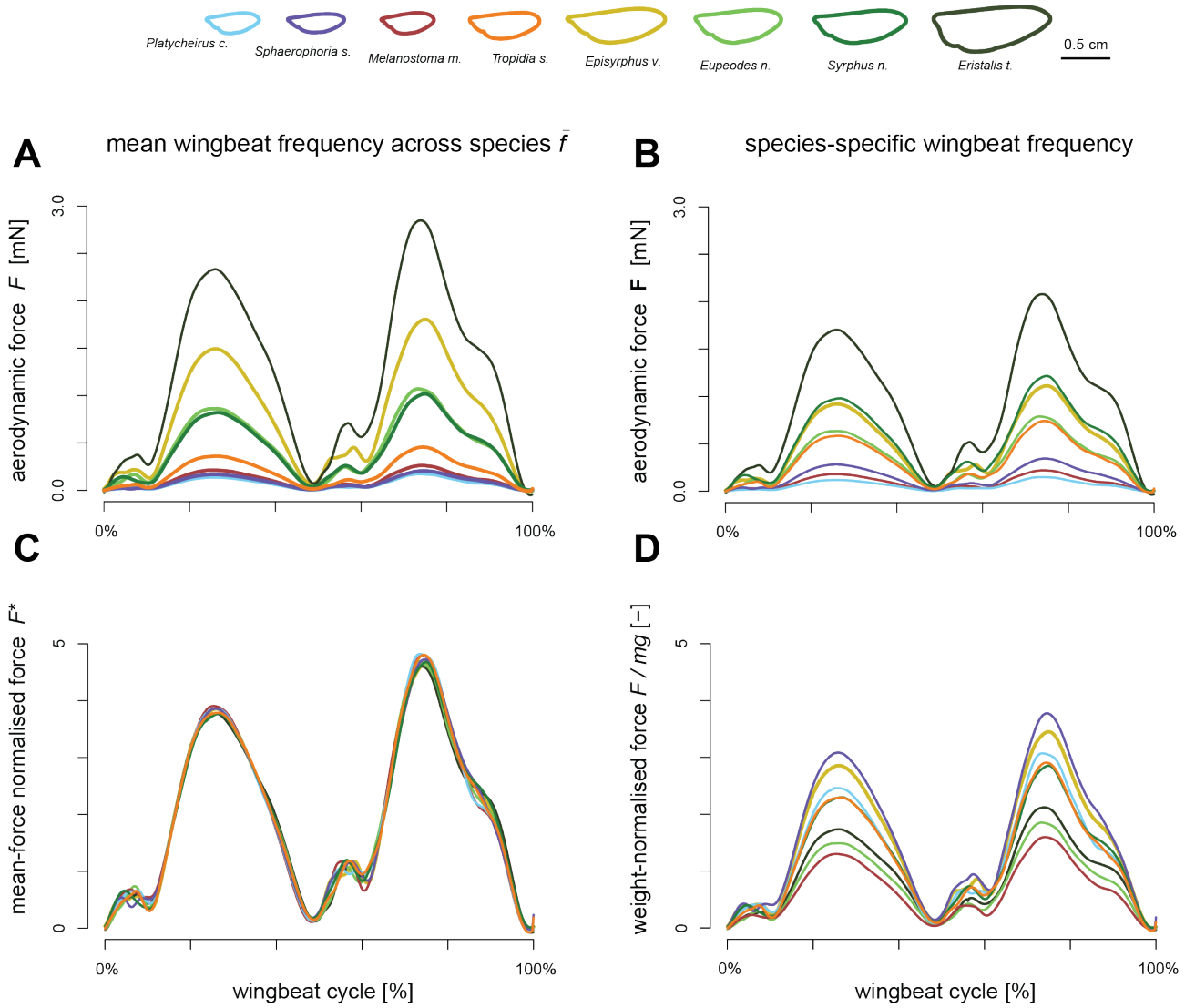

Figure S6. Temporal dynamic of the vertical aerodynamic forces produced during the wingbeat of the eight studied hoverfly species, estimated using Computation Fluid Dynamics (CFD) simulations. Data for the eight species are colour-coded according to the legend on the top. All simulations were run with the mean wingbeat kinematics of all hoverflies combined (Fig 6A,B), but with species-specific wing morphology (see legend on top). The aerodynamic forces in the different panels are scaled and normalized using four different methods: (A) aerodynamic forces as directly estimated using the CFD simulations, and where all wings operate at the mean wingbeat frequency of all hoverflies ($\bar{f}$); (B) aerodynamic forces as produced by each hoverfly beating its wings at the species-specific wingbeat frequency *f*; (C) aerodynamic forces normalized with its wingbeat-average force, $F^* = F/\bar{F}$; (D) aerodynamic forces produced using the species-specific wingbeat frequency, and normalized with the mean weight of the specific hoverfly species *F/mg*.

Table S1. Results of ANOVAs testing the effect of sex and species on wing morphology parameters.

Variable	Factor	*F*-value	*P*-value
Body mass *m*			
	sex	4.061	**0.047**
	species	53.897	**<0.001**
Second-moment-of-area S_2			
	sex	11.592	**0.001**
	species	38.489	**<0.001**
Wingspan *R*			
	sex	0.334	0.564
	species	67.411	**<0.001**
Wing chord $\bar{c}$			
	sex	6.202	**0.014**
	species	71.933	**<0.001**
Normalized second- moment of-area S_2*			
	sex	2.719	0.103
	species	21.231	**<0.001**

Bold indicates statistical significance

Table S2. Phylogenetic signal computed on morphological and flight traits. Species number in the morphology and flight dataset is 28 and 8, respectively.

Morphological traits			**Flight traits**		
	Blomberg's K	P		Blomberg's K	P
Body mass m	0.81	**0.004**	Wingbeat frequency f	0.66	0.696
Wingspan R	0.66	**0.005**	Stroke amplitude A_ϕ	0.91	0.187
Wing chord $\bar{c}$	0.72	**0.004**	Wing angular speed $\bar{\omega}$	0.89	0.235
Second moment of area S_2	0.59	0.071	Angle-of-attack $\bar{\alpha}$	1.01	0.145
Normalized second moment of area S_2 *	0.88	**0.004**			

Bold indicates statistical significance.

Table S3. Results from multiple regressions testing correlations between the wingbeat kinematics parameters and body kinematics, expressed by flight speed and climb angle.

	Flight speed		Climb angle	
	t value	P	t value	P
Wingbeat frequency f	1.976	0.057	-0.401	0.691
Stroke amplitude A_ϕ	-0.037	0.971	0.602	0.552
Wing angular speed $\bar{\omega}$	2.331	**0.026**	0.499	0.621
Angle-of-attack $\bar{\alpha}$	0.721	0.477	-0.451	0.655

Bold indicates statistical significance.

Table S4. Results of phylogenetic generalized least square (PGLS) regressions of additional wingbeat kinematic parameters against body mass.

	n	P	R^2	Intercept	Scaling factor estimate [95% C.I.]
Rotation amplitude A_θ	8	0.301	0.25	4.692	0.016 [-0.011 – 0.044]
Deviation amplitude A_η	8	0.942	0.07	0.492	0.022 [-0.551 – 0.595]
Peak stroke rate $\dot{\varphi}_{peak}$	8	0.201	0.11	11.178	-0.103 [-0.244 – 0.037]
Peak rotation rate $\dot{\theta}_{peak}$	8	0.901	0.03	11.488	0.014 [-0.203 – 0.232]
Peak deviation rate $\dot{\eta}_{peak}$	8	0.247	0.14	10.308	-0.216 [-0.546 – 0.114]